Microscopic Analysis of the Uplink Interference in FDMA Small Cell Networks

Ming Ding, *Member, IEEE*, David López-Pérez, *Member, IEEE*,
Guoqiang Mao, *Senior Member, IEEE*, Zihuai Lin, *Senior Member, IEEE*

***Abstract*—In this paper, we analytically derive an upper bound on the error in approximating the uplink (UL) single-cell interference by a lognormal distribution in frequency division multiple access (FDMA) small cell networks (SCNs). Such an upper bound is measured by the Kolmogorov–Smirnov (KS) distance between the actual cumulative density function (CDF) and the approximate CDF. The lognormal approximation is important because it allows tractable network performance analysis. Our results are more general than the existing works in the sense that we do not pose any requirement on (i) the shape and/or size of cell coverage areas, (ii) the uniformity of user equipment (UE) distribution, and (iii) the type of multi-path fading. Based on our results, we propose a new framework to directly and analytically investigate a complex network with practical deployment of multiple BSs placed at irregular locations, using a power lognormal approximation of the aggregate UL interference. The proposed interference analysis is particularly useful for the 5th generation (5G) systems with more general cell deployment and UE distribution beyond the widely used Poisson distribution.**

***Index Terms*—uplink, interference analysis, frequency division multiple access (FDMA), small cell networks (SCNs), approximation, Gaussian, sum lognormal, power lognormal.**

I. INTRODUCTION

Small cell networks (SCNs) have been identified as one of the key enabling technologies in the 5th generation (5G) networks [1]. In this context, new and more powerful network performance analysis tools are being developed to gain a deep understanding of the performance implications that SCNs bring about. These new network performance analysis tools are significantly different from traditional ones used to study just a few macrocells only, and can be broadly classified into two large groups, i.e., macroscopic analysis and microscopic analysis [2-10].

The macroscopic analysis assumes that both user equipments (UEs) and base stations (BSs) are randomly deployed in the network, often following the homogeneous Poisson distribution, and usually tries to derive the signal-to-interference-plus-noise ratio (SINR) distribution of UEs and other performance metrics such as the coverage probability and the area spectral efficiency (ASE) [2,3]. In contrast, the microscopic analysis is often conducted assuming that UEs are randomly placed and BSs are deterministically deployed, i.e., the BS positions are known [4-10].

It is important to note that these two analyses are related to each other. The average performance of microscopic analyses conducted over a large number of realizations of random BS deployments should be equal to that of the macroscopic analysis, when the examined realizations of the deterministic BS deployments follow the assumption on the BS deployment used in the macroscopic analysis.

The microscopic analysis is important because it allows for a network-specific study and optimization, e.g., optimizing the parameters of UL power control [8] and performing per-cell loading balance in a specific SCN [9]. In contrast, the macroscopic analysis investigates network performance at a high level by averaging out all the possible BS deployments [2,3]. Generally speaking, the microscopic analysis gives more targeted results for specific networks than the macroscopic analysis, while the macroscopic analysis gives a general picture of the network performance.

In this paper, we focus on the microscopic analysis. In particular, we consider an uplink (UL) frequency division multiple access (FDMA) SCN, which has been widely adopted in the 4th generation (4G) networks, i.e., the UL single-carrier FDMA (SC-FDMA) system in the 3rd Generation Partnership Project (3GPP) Long Term Evolution (LTE) networks [11] and the UL orthogonal FDMA (OFDMA) system in the Worldwide Interoperability for Microwave Access (WiMAX) networks [12].

For the UL microscopic analysis, the existing works use

- Approach 1, which provides closed-form expressions but complicated analytical results for a network with *a small number of interfering cells and each cell has a regularly-shaped coverage area*, e.g., a disk or a hexagon [4]. In [4], the authors considered a single UL interfering cell with a disk-shaped coverage area and presented closed-form expressions for the UL interference considering both path loss and shadow fading.
- Approach 2, which first analyzes the UL interference and then makes an empirical assumption on the UL

Manuscript received xxx xx, 2015; revised xxx xx, 2015; accepted xxx xx, 2016. Preliminary results related to this paper were presented at IEEE Globecom Conference 2015 [10]. The associate editor coordinating the review of this paper and approving it for publication was x. xxxx.

Ming Ding is with Data61, Sydney, Australia (e-mail: Ming.Ding@nicta.com.au).

David López-Pérez is with Bell Labs, Nokia, Dublin, Ireland (email: dr.david.lopez@ieee.org).

Guoqiang Mao is with (1) the School of Computing and Communication, The University of Technology Sydney, Australia, (2) Data61, Sydney, Australia, (3) School of Electronic Information & Communications, Huazhong University of Science & Technology, Wuhan, China, and (4) School of Information and Communication Engineering, Beijing University of Posts and Telecommunications, Beijing, China (e-mail: g.mao@ieee.org). Guoqiang Mao's research is supported by Australian Research Council (ARC) Discovery projects DP110100538 and DP120102030 and Chinese National Science Foundation project 61428102.

Zihuai Lin is with the School of Electrical and Information Engineering, The University of Sydney, Australia (e-mail: zihuai.lin@sydney.edu.au).

Digital Object Identifier xx.xxxx/TWC.2016.xxxxxxx

interference distribution, and on that basis derives analytical results for a network with *multiple interfering cells, whose BSs are placed on a regularly-shaped lattice*, e.g., a hexagonal lattice [5]-[7]. Specifically, in [5] and [6], the authors showed that the lognormal distribution better matches the distribution of the uplink interference in a hexagonal cellular layout than the conventionally assumed Gaussian distribution. In [7], the authors assumed that the uplink interference in hexagonal grid based OFMDA cellular networks should follow a lognormal distribution. Such assumption was verified via simulation.

- Approach 3, which conducts system-level simulations to directly obtain empirical results for a complex network with *practical deployment of multiple cells, whose BSs are placed at irregular locations* [1], [8], [9]. In particular, the authors of [1], [8], [9] conducted system-level simulations to investigate the network performance of SCNs in existing 4G networks and in future 5G networks.

Obviously, Approach 1 and Approach 3 lack generality and analytical rigor, respectively. Regarding Approach 2, it has been a number of years since an empirical conjecture was extensively used in performance analysis, which stated that the UL inter-cell interference with *disk-shaped* coverage areas and uniform UE distributions could be well approximated by a lognormal distribution in code division multiple access (CDMA) SCNs [5], [6] and in FDMA SCNs [7]. This conjecture is important since the lognormal approximation of the interference distribution allows tractable network performance analysis. However, up to now, it is still unclear *how accurate* this lognormal approximation is.

In this paper, we aim to answer this fundamental question, thus making a significant contribution to constructing a formal tool for the microscopic analysis of network performance. Note that in our previous work [10], we investigated an upper bound on the error of this lognormal approximation under the assumptions of uniform UE distribution and Rayleigh multi-path fading. In this paper, we will largely extend our previous work by presenting a new and tighter upper bound on the error of this approximation, and further remove the requirement on the uniformity of UE distribution and the type of multi-path fading. In particular, we will focus on the analysis of UL inter-cell interference. This interference analysis is important because it paves way to the analyses of SINR, as well as other performance metrics such as the coverage probability and the ASE. The contributions of this paper are as follows:

1) Our work analytically derives an upper bound on the error in approximating the UL single-cell interference in FDMA SCNs by a lognormal distribution. Such error is measured by the Kolmogorov–Smirnov (KS) distance [13] between the actual cumulative density function (CDF) and the approximate CDF.
2) Unlike the existing works on the microscopic analysis, e.g., [4-11], our work does not pose any requirement on *(i)* the shape and/or size of cell coverage areas, *(ii)* the uniformity of UE distribution, and *(iii)* the type of multi-path fading. Thus, our proposed framework is more general and useful for network performance analysis.
3) Based on our work, a new approach can be established to fill an important theoretical gap in the existing microscopic analysis of network performance, which either assumes very simple BS deployments or relies on intricate simulations. Such new approach allows us to directly investigate a complex network with *practical deployment of multiple BSs placed at irregular locations*, while retaining mathematical rigor in the analysis. In order to do that, we first verify the accuracy of the approximated UL interference distribution for each small cell, and then we approximate the aggregate UL interference by a power lognormal distribution. Specifically, the CDF of a power lognormal distribution is a power function of the CDF of a lognormal distribution, which enables the microscopic analysis on the UE SINR distribution in our future work.

The remainder of the paper is structured as follows. In Section II, the network scenario and the system model are described. In Section III, our approach of studying the UL inter-cell interference in FDMA SCNs is presented, followed by the validation of our results via simulations in Section IV. Finally, the conclusions are drawn in Section V.

II. NETWORK SCENARIO AND SYSTEM MODEL

In this paper, we consider UL transmissions and assume that in one frequency resource block (RB) and in a given time slot, only *one* UE is scheduled by each small cell BS to perform an UL transmission, which is a reasonable assumption in line with the 4G networks, i.e., the UL SC-FDMA system in the LTE networks [11] and the UL OFDMA system in the WiMAX networks [12]. We assume that each small cell has at least one associated UE. Small cell BSs having no UE do not contribute to the uplink interference analyzed in this paper, thereby can be ignored.

Regarding the network scenario, we consider a SCN with multiple small cells operating on the same carrier frequency. Fig. 1 illustrates this SCN, which consists of B small cells, each of which is managed by a BS. The network includes one small cell of interest denoted by C_1 and $B-1$ interfering small cells denoted by $C_b, b \in \{2, \ldots, B\}$. We focus on a particular frequency RB, and denote by K_b the active UE associated with small cell C_b using such frequency RB. Moreover, we denote by R_b *the coverage area* of small cell C_b, in which its associated UEs are randomly distributed. Note that the coverage areas of adjacent small cells may overlap due to the arbitrary shape and size of $\{R_b\}, b \in \{2, \ldots, B\}$.

The distance (in km) from the BS of C_b to the BS of C_1, $b \in \{1, \ldots, B\}$, and the distance from UE K_b to the BS of C_m, $b, m \in \{1, \ldots, B\}$, are denoted by D_b and d_{bm}, respectively. In this paper, we consider a deterministic deployment of BSs, and thus the set $\{D_b\}$ is assumed to be known. However, UE K_b is assumed to be randomly distributed in R_b with a distribution function $f_{Z_b}(z), z \in R_b$. Hence, d_{bm} is a random variable (RV), whose distribution cannot be readily expressed in an analytical form due to the arbitrary shape and size of R_b, and the arbitrary form of $f_{Z_b}(z)$. Unlike the existing works, e.g., [2-8], that only treat

This article has been accepted for publication in a future issue of this journal, but has not been fully edited. Content may change prior to final publication. Citation information: DOI 10.1109/TWC.2016.2538261, IEEE Transactions on Wireless Communications

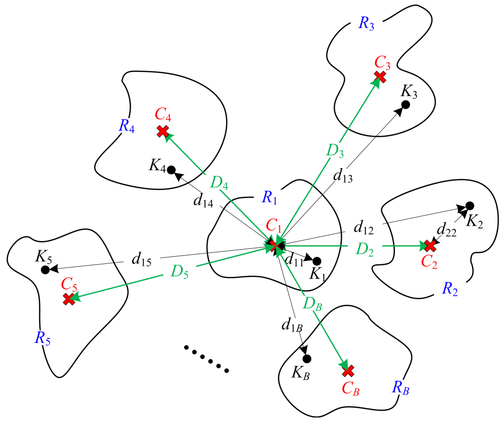

Fig. 1. A schematic model of the considered SCN.

uniform UE distributions, in this work we investigate a general probability density function (PDF) of UE distribution denoted by $f_{Z_b}(z)$, which satisfies $0 < f_{Z_b}(z) < +\infty, z \in R_b$, and its integral over R_b equals to one, i.e., $\int_{R_b} f_{Z_b}(z)\,dz = 1$.

In the following, we present the modeling of path loss, shadow fading, UL transmission power, and multi-path fading, respectively.

Based on the definition of d_{bm}, *the path loss* (in dB) from UE K_b to the BS of C_m is modeled as

$$L_{bm} = A + \alpha \log_{10} d_{bm}, \tag{1}$$

where A is the path loss at the reference distance of $d_{bm} = 1$ and α is the path loss exponent. In practice, A and α are constants obtainable from field tests [14]. Note that L_{bm} is a RV due to the randomness of d_{bm}.

The shadow fading (in dB) from UE K_b to the BS of C_m is denoted by S_{bm}, and it is usually modeled as a zero-mean Gaussian RV because the linear-scale value of S_{bm} is commonly assumed to follow a lognormal distribution [14]. Hence, in this paper, we model S_{bm} as an independently and identically distributed (i.i.d.) zero-mean Gaussian RV with variance σ^2_{Shad}, denoted by $S_{bm} \sim \mathcal{N}\left(0, \sigma^2_{\mathrm{Shad}}\right)$.

The UL transmission power (in dBm) of UE K_b is denoted by P_b. In practice, P_b is usually subject to a semi-static power control (PC) mechanism[1], e.g., the fractional pathloss compensation (FPC) scheme [14]. Based on this FPC scheme, P_b in dBm is modeled as

$$P_b = P_0 + \eta \left(L_{bb} + S_{bb}\right), \tag{2}$$

where P_0 is the target received power at the BS in dBm on the considered frequency RB, $\eta \in (0, 1]$ is the FPC factor, L_{bb} has been defined in (1), and $S_{bb} \sim \mathcal{N}\left(0, \sigma^2_{\mathrm{Shad}}\right)$ has been discussed above.

The multi-path fading channel from UE K_b to the BS of C_m is denoted by $\mathbf{h}_{bm} \in \mathbb{C}$, where we assume that each UE and each BS are equipped with one omni-directional antenna. In this paper, we consider a general type of multi-path fading by assuming that the effective channel gain (in dB) associated with $\mathbf{h}_{bm}$ is defined as $10\log_{10}|\mathbf{h}_{bm}|^2$ and denoted by H_{bm}, which follows an i.i.d. distribution with the PDF of $f_H(h)$. For example, $|\mathbf{h}_{bm}|^2$ can be characterized by an exponential distribution in case of Rayleigh fading [15].

For clarity, the defined RVs in our system model are summarized in Table I.

III. ANALYSIS OF THE UL INTERFERENCE DISTRIBUTION

Based on the definition of RVs discussed in Section II, *the UL received interference power* (in dBm) from UE K_b to the BS of C_1 can be written as

$$\begin{aligned} I_b &\overset{(a)}{=} P_b - L_{b1} - S_{b1} + H_{b1} \\ &= P_0 + (\eta L_{bb} - L_{b1}) + (\eta S_{bb} - S_{b1}) + H_{b1} \\ &\triangleq (P_0 + L + S) + H_{b1}, \\ &\triangleq I_b^{(1)} + H_{b1}, \end{aligned} \tag{3}$$

where (2) is plugged into the step (a) of (3), and L and S are defined as $L \triangleq (\eta L_{bb} - L_{b1})$ and $S \triangleq (\eta S_{bb} - S_{b1})$, respectively. Besides, the first part of I_b is further defined as $I_b^{(1)} \triangleq (P_0 + L + S)$. Apparently, L and S are independent RVs. Since S_{bb} and S_{b1} $(b \in \{2, \ldots, B\})$ are i.i.d. zero-mean Gaussian RVs, it is easy to show that S is also a Gaussian RV, whose mean and variance are

$$\begin{cases} \mu_S = 0 \\ \sigma^2_S = \left(1 + \eta^2\right)\sigma^2_{\mathrm{Shad}} \end{cases}. \tag{4}$$

From the definition of I_b in (3), *the aggregate interference power* (in mW) from all interfering UEs to the BS of C_1 can be written as

$$I^{\mathrm{mW}} = \sum_{b=2}^{B} 10^{\frac{1}{10} I_b}. \tag{5}$$

In the following subsections, we will analyze the distribution of I^{mW} in three steps:

- First, we investigate the distribution of $I_b^{(1)}$ shown in (3), and approximate such distribution by a Gaussian distribution. The upper-bound of the approximation error measured by the KS distance [13] is derived in closed-form expressions.
- Second, we analyze the sum of RVs $\left(I_b^{(1)} + H_{b1}\right)$ shown in (3) and further approximate such distribution by another Gaussian distribution. The upper-bound of the approximation error measured by the KS distance [13] is derived in closed-form expressions.
- Third, we show that the distribution of I^{mW} can be well approximated by a power lognormal distribution, i.e.,

---

[1] Note that in practice P_b is also constrained by the maximum value of the UL power, denoted by $P_{\max}$ at the UE. However, the power constraint is a minor issue for UEs in SCNs since they are generally not power-limited due to the close proximity of a UE and its associated SCN BS. For example, it is recommended in [14] that $P_{\max}$ is smaller than the SCN BS downlink (DL) power by only 1dB, which grants a similar outreach range of signal transmission for the BS and the UE. Therefore, the UL power limitation is a minor issue as long as the UE is able to connect with the serving BS in the DL. If the UE cannot establish a DL connection with the serving BS, then it is not very meaningful to consider the UL power constraint issue since the UL connection cannot exist without the assistance of the DL control signaling. For the sake of tractability, in this paper, we model P_b as (2), which has been widely adopted in the literature [3,6-8,11]. Note that the power constraint issue should be considered for the macrocell networks, where the maximum transmit power of a BS is at least 20dB higher than $P_{\max}$, and a UE may be very likely to experience power back-off [14] at cell-edge areas.

Table I
DEFINITION OF RVS.

RV	Description	Distribution
Z_b	The position of K_b in R_b	The PDF is $f_{Z_b}(z), z \in R_b$
d_{bm}	The distance (in km) from K_b to C_m	Related to $f_{Z_b}(z)$, R_b and D_b
L_{bm}	The path loss (in dB) from K_b to C_m	Related to $f_{Z_b}(z)$, R_b and D_b
S_{bm}	The shadow fading (in dB) from K_b to C_m	i.i.d. $\mathcal{N}\left(0, \sigma_{\text{Shad}}^2\right)$
H_{bm}	The channel gain (in dB) from K_b to C_m	i.i.d. distribution with the PDF of $f_H(h)$
P_b	The UL transmission power (in dBm) of K_b	Related to $f_{Z_b}(z)$, R_b and S_{bb}

with the CDF being a power function of the CDF of a lognormal distribution.

A. The Distribution of $I_b^{(1)}$ in (3)

Considering the complicated mathematical form of L in (3), we can find that the PDF of L is generally not tractable because L is a RV with respect to d_{bb} and d_{b1}, which jointly depends on the arbitrary shape/size of R_b and the arbitrary form of $f_{Z_b}(z)$. Specifically, for any point $z \in R_b$, d_{bb} and d_{b1} are geometric functions of z, and the probability density of z is $f_{Z_b}(z)$. Despite the intractable nature of L, we will show that $I_b^{(1)}$ can still be approximated by a Gaussian RV with bounded approximation errors. In more detail, we investigate an upper bound on the error in approximating the sum of an arbitrary RV and a Gaussian RV, i.e., $(L+S)$, by another Gaussian RV. To that end, we denote by μ_L and σ_L^2 the mean and variance of L respectively. Moreover, we define two zero-mean RVs as $\tilde{L} = L - \mu_L$ and $\tilde{S} = S - \mu_S$, respectively. As a result, $I_b^{(1)}$ in (3) can be re-written as

$$I_b^{(1)} = \left(\tilde{L} + \tilde{S}\right) + \left(P_0 + \mu_L + \mu_S\right). \tag{6}$$

In (6), $\tilde{L}$ is still not tractable. However, since $\tilde{S}$ is a Gaussian RV with a relatively large variance of $\left(1+\eta^2\right)\sigma_{\text{Shad}}^2$ shown in (4), we propose that $\left(\tilde{L}+\tilde{S}\right)$ can be approximated by a Gaussian RV with bounded approximation errors. As a result, if $\left(\tilde{L}+\tilde{S}\right)$ can be well approximated by a Gaussian RV, then $I_b^{(1)}$ can also be well approximated by the same Gaussian RV with an offset $\left(P_0 + \mu_L + \mu_S\right)$.

1) The Distribution of $\left(\tilde{L}+\tilde{S}\right)$ in (6): For the convenience of mathematical expression, the mean, the variance, the 3rd moment and the 4th moment of $\tilde{L}$ are denoted by $\mu_{\tilde{L}} = 0$, $\sigma_{\tilde{L}}^2 = \sigma_L^2$, $\rho_{\tilde{L}}^{(3)}$ and $\rho_{\tilde{L}}^{(4)}$, respectively. Besides, considering (4), the mean and the variance of $\tilde{S}$ are denoted by $\mu_{\tilde{S}} = 0$, $\sigma_{\tilde{S}}^2 = \sigma_S^2$, respectively. Moreover, we define $\tilde{G} \triangleq \tilde{L} + \tilde{S}$ and denote the PDF of $\tilde{L}$ by $f_{\tilde{L}}(l)$.

In order to quantify the approximation error between the distribution $\tilde{G}$ and its approximate Gaussian distribution, we invoke the following definition on the KS distance between two CDFs [13].

Definition 1. Suppose that the CDFs of RVs X and $\hat{X}$ are $F_X(x)$ and $F_{\hat{X}}(x)$, respectively. Then the KS distance between $F_X(x)$ and $F_{\hat{X}}(x)$ is defined as

$$KS(X,Y) = \sup_{x\in\mathbb{R}} \left|F_X(x) - F_{\hat{X}}(x)\right|. \tag{7}$$

The KS distance is a widely used metric to measure the difference between two CDFs. Based on Definition 1, we present Theorem 2 in the following to bound the KS distance between the CDF of $\tilde{G}$ and that of the corresponding approximate zero-mean Gaussian RV with a variance of $\left(\sigma_L^2 + \sigma_S^2\right)$.

Theorem 2. *Considering the zero-mean RV $\tilde{G} = \tilde{L} + \tilde{S}$ given by (6), the KS distance between the CDF of $\tilde{G}$ and that of the corresponding approximate zero-mean Gaussian RV with a variance of $\left(\sigma_L^2 + \sigma_S^2\right)$ is bounded by*

$$\sup_{g\in\mathbb{R}} \left| F_{\tilde{G}}(g) - \Phi\left(\frac{g}{\sqrt{\sigma_L^2+\sigma_S^2}}\right)\right| \le \max\left\{\varepsilon_1 + \varepsilon_2,\ \varepsilon_3\right\}, \tag{8}$$

where $F_{\tilde{G}}(g)$ and $\Phi(\cdot)$ are respectively the CDF of $\tilde{G}$ and the CDF of the standard normal distribution, and $\max\{x,y\}$ *extracts the larger value between x and y.*

Moreover, ε_1 in (8) is expressed as

$$\begin{aligned}\varepsilon_1 \ = \ & \frac{1}{2}\delta_1(\omega,p)\frac{1}{k_2^2} + \frac{1}{2}\delta_0\left(\omega, p, \frac{(k_1+k_2)\sqrt{\sigma_L^2+\sigma_S^2}}{\sqrt{2}\sigma_S}\right) \\ & + \frac{1}{2}\delta_0\left(\frac{\omega\sqrt{\sigma_L^2+\sigma_S^2}}{\sigma_S}, p, \frac{k_1}{\sqrt{2}}\right),\end{aligned} \tag{9}$$

where ω, p, k_1 and k_2 are positive scalars. Besides, $f_{\tilde{L}}(l)$ is the PDF of $\tilde{L}$, and $\delta_0(\omega,p,k)$ and $\delta_1(\omega,p,k)$ are given by

$$\begin{cases}\delta_0(\omega,p,k) = \frac{2}{\sqrt{\pi}\omega}\mathit{erfc}\left((2p+1)\omega\right) + \mathit{erfc}\left(\frac{\pi}{2\omega} - k\right) \\ \delta_1(\omega,p) = \frac{2}{\sqrt{\pi}\omega}\mathit{erfc}\left((2p+1)\omega\right) + 2\end{cases}, \tag{10}$$

where erfc$(\cdot)$ is the complementary error function [15].

In addition, ε_2 in (8) is given by

$$\varepsilon_2 = \frac{2}{\pi}\sum_{n=1, n\ odd}^{2p-1} \left|\upsilon_n - \hat{\upsilon}_n\right|, \tag{11}$$

where $\upsilon_n = \frac{1}{n}\exp\left(-\frac{n^2\omega^2}{2}\right)\varphi_{\tilde{L}}\left(-\frac{n\omega}{\sigma_S}\right)$, $\hat{\upsilon}_n = \frac{1}{n}\exp\left(-\frac{n^2\omega^2}{2}\left(\frac{\sigma_L^2+\sigma_S^2}{\sigma_S^2}\right)\right)$, and $\varphi_{\tilde{L}}(t)$ is the characteristic function [16] of $f_{\tilde{L}}(l)$.

Finally, ε_3 in (8) is expressed as

$$\varepsilon_3 = \frac{1}{k_1^2} + \frac{1}{2}\mathit{erfc}(k_1). \tag{12}$$

Proof: See Appendix A. ■

Theorem 2 is useful to quantify the maximum error of approximating $\tilde{G}$ by a Gaussian RV. From the proof in Appendix A, it can be seen that

- ε_1 in (8) is caused by the residual errors from the p-truncated Fourier series expansion of $\operatorname{erfc}(\cdot)$, where p is the number of the truncated terms.
- ε_2 in (8) is the major part of the approximation error caused by approximating $\tilde{G}$ by a Gaussian RV.
- ε_3 in (8) measures the asymptotic difference between $F_{\tilde{G}}(g)$ and $\Phi\left(\frac{g}{\sqrt{\sigma_L^2+\sigma_S^2}}\right)$ for $|g| \geq k_1\sqrt{\sigma_L^2+\sigma_S^2}$, where k_1 takes a large value to show the asymptotic behavior of the interested CDFs.

To obtain some insights on the typical values of ε_1, ε_2 and ε_3, we should first discuss the appropriate choices of the values of ω, p, k_1 and k_2. To that end, we have the following remarks.

Remark 1: ω is the fundamental frequency of the Fourier series expansion of $\operatorname{erfc}(\cdot)$, and thus it should satisfy the condition that $\frac{1}{\omega}$ is much larger than the spread of x in $\operatorname{erfc}(x)$ [15], which can be estimated to be in the range of $[-5,5]$ because $|\operatorname{erfc}(-\infty)-\operatorname{erfc}(-5)| = 1.54\times10^{-12}\approx 0$ and $|\operatorname{erfc}(+\infty)-\operatorname{erfc}(5)| = 1.54\times10^{-12}\approx 0$. Therefore, $\frac{1}{\omega}$ should be much larger than 10 due to the range of $[-5,5]$. We propose that a typical value of $\frac{1}{\omega}$ could be 1000, i.e., $\omega = 0.001$.

Remark 2: p is the number of the truncated terms in the p-truncated Fourier series expansion of $\operatorname{erfc}(\cdot)$, and thus it should be sufficiently large to make the residual error caused by the truncation of the Fourier series expansion sufficiently small. The part of the residual error that is related to p is expressed as $\tilde{\delta}(\omega,p) = \frac{2}{\sqrt{\pi}\omega}\operatorname{erfc}((2p+1)\omega)$ in (10). From this expression, we can see that p should be larger than $\frac{2}{\omega}$ to make $\tilde{\delta}(\omega,p)$ sufficiently small, because $\operatorname{erfc}\left(\left(2\times\frac{2}{\omega}+1\right)\omega\right) = 1.4\times10^{-8}$ when $\omega = 0.001$. We propose that a typical value of p could be $\frac{4}{\omega}$, which equals to 4000 when $\omega = 0.001$. The corresponding $\tilde{\delta}(\omega,p)$ will then drop to a small value of 1.1×10^{-27}.

Remark 3: Since k_1 is related to the asymptotic behavior of $F_{\tilde{G}}(g)$ and $\Phi\left(\frac{g}{\sqrt{\sigma_L^2+\sigma_S^2}}\right)$ when $|g| \geq k_1\sqrt{\sigma_L^2+\sigma_S^2}$, k_1 should be sufficiently large to make ε_3 sufficiently small. We propose that the typical value of k_1 should be at least 100 to achieve an ε_3 as small as 1.0×10^{-4}, which corresponds to a small error of ±0.01 percentile. As will be shown in Section IV, k_1 is set to 500, thus having $\varepsilon_3 = 4\times10^{-6}$, which is confirmed to be always smaller than ε_2 in our numerical results.

Remark 4: As discussed in Appendix A, the introduction of k_2 is to facilitate the bounding of the integral over l from $-\infty$ to $+\infty$. From (9), the first term of (9), i.e., $\frac{1}{2}\delta_1(\omega,p)\frac{1}{k_2^2}$, dominates ε_1 because $\delta_0(\omega,p,k)$ is a very small value with appropriate choices of ω, p, k_1 and k_2. For example, as discussed above, if we choose $\omega = 0.001$, $p = 4000$, $k_1 = k_2 = 500$, and $\sigma_L = \sigma_S$, then the first term of (9) becomes 4×10^{-6}, while the sum of the remaining terms is merely 6.3×10^{-27}. We propose that the typical value of k_2 should be at least 100 to achieve an ε_1 as small as 1.0×10^{-4}, which corresponds to a small error of ±0.01 percentile. As will be shown in Section IV, k_2 is set to 500, this having $\varepsilon_1 = 4\times10^{-6}$, which is confirmed to be always smaller than ε_2 in our numerical results.

Considering the expressions of ε_1 and ε_3 shown in (9) and (12), respectively, if we investigate the special case where $k_1 = k_2$, then it is straightforward to get that $\varepsilon_1 > \varepsilon_3$. Hence, we propose the following corollary to simplify Theorem 2.

Corollary 3. *When $k_1 = k_2$, the KS distance between the CDF of $\tilde{G}$ and that of the corresponding approximate zero-mean Gaussian RV with a variance of $\left(\sigma_L^2+\sigma_S^2\right)$ is bounded by*

$$\sup_{g\in\mathbb{R}}\left|F_{\tilde{G}}(g)-\Phi\left(\frac{g}{\sqrt{\sigma_L^2+\sigma_S^2}}\right)\right| \leq \varepsilon_1+\varepsilon_2. \qquad (13)$$

Note that compared with (8), ε_3 does not exist in the right-hand side of (13), which largely simplifies our analysis and discussion. Therefore, in the sequel we will only consider (13) to quantify the maximum error of approximating $\tilde{G}$ by a Gaussian RV.

With the discussed typical values of ω, p, k_1 and k_2, we can see that ε_1 in (13) can be controlled to be as small as 4×10^{-6}, which leaves ε_2 as the major contributor to the derived upper-bound of the KS distance. We will briefly discuss the calculation of ε_2 in the next subsection. Note that further optimization of k_1 and k_2 to reduce ε_3 and ε_1 even below 4×10^{-6} is possible. However, such optimization has a marginal impact on the derived upper bound of the approximation error because ε_2 is independent of k_1 and k_2.

With Theorem 2 and Corollary 3 characterizing the upper bound of the approximation error, we propose to approximate $I_b^{(1)}$ in (6) by a Gaussian RV G_b, whose mean and variance can be computed by

$$\begin{cases}\mu_{G_b} = P_0+\mu_L+\mu_S\\ \sigma_{G_b}^2 = \sigma_L^2+\sigma_S^2\end{cases}. \qquad (14)$$

2) The Calculation of ε_2 in (11): For each small cell C_b, considering the definition of L and $\tilde{L}$ presented in (3) and (6), respectively, we can evaluate $\varphi_{\tilde{L}}\left(-\frac{n\omega}{\sigma_S}\right)$ for each small cell C_b as

$$\begin{aligned}&\varphi_{\tilde{L}}\left(-\frac{n\omega}{\sigma_S}\right)\\ &= \int_{-\infty}^{+\infty}\exp\left(-\mathrm{j}\frac{n\omega l}{\sigma_S}\right)f_{\tilde{L}}(l)\,dl\\ &= \int_{R_b}\exp\left(-\mathrm{j}n\omega\frac{L(z)-\mu_L}{\sigma_S}\right)f_{Z_b}(z)\,dz\\ &\overset{(a)}{=} \int_{R_b}\exp\left(-\mathrm{j}n\omega\frac{\eta L_{bb}(z)-L_{b1}(z)-\mu_L}{\sigma_S}\right)f_{Z_b}(z)\,dz, \qquad (15)\end{aligned}$$

where (1) should be inserted into the step (a) of (15) and μ_L is the mean of L.

With the result of $\varphi_{\tilde{L}}\left(-\frac{n\omega}{\sigma_S}\right)$, we can then compute ε_2 according to its definition in (11).

B. The Distribution of I_b in (3)

Having approximated $I_b^{(1)}$ by a Gaussian RV G_b, we can approximate (3) as

$$I_b \approx G_b + H_{b1}. \qquad (16)$$

It is interesting to note that, similar to $I_b^{(1)}$ in (3), the approximate expression of I_b in (16) also contains a Gaussian RV G_b and an arbitrary RV H_{b1} with the PDF of $f_H(h)$.

Based on the above observation, we propose to reuse Theorem 2 and Corollary 3 to quantify the error in approximating I_b in (16) by an another Gaussian RV. To that end, similar to (6), we define two zero-mean RVs as $\tilde{G}_b = G_b - \mu_{G_b}$ and $\tilde{H}_{b1} = H_{b1} - \mu_{H_{b1}}$, where μ_{G_b} and $\mu_{H_{b1}}$ are the means of G_b and H_{b1}, respectively. Besides, the variance of G_b and H_{b1} are denoted by $\sigma^2_{G_b}$ and $\sigma^2_{H_{b1}}$, respectively. As a result, we can re-formulate (16) as

$$I_b \approx \left(\tilde{G}_b + \tilde{H}_{b1}\right) + \left(\mu_{G_b} + \mu_{H_{b1}}\right). \tag{17}$$

Next, we approximate $\left(\tilde{G}_b + \tilde{H}_{b1}\right)$ by a Gaussian RV, and it follows that I_b can also be approximated by the same Gaussian RV with an offset $\left(\mu_{G_b} + \mu_{H_{b1}}\right)$.

1) The Distribution of $\left(\tilde{G}_b + \tilde{H}_{b1}\right)$ in (17): We propose to approximate $\left(\tilde{G}_b + \tilde{H}_{b1}\right)$ as a zero-mean Gaussian RV with a variance of $\sigma^2_{G_b} + \sigma^2_{H_{b1}}$, then from Corollary 3, the error measured by the KS distance between the actual CDF and the approximate CDF can be upper-bounded by $\varepsilon_1' + \varepsilon_2'$, where ε_1' and ε_2' are computed using (9) and (11), respectively, with the following RV changes,

$$\begin{cases} \varepsilon_1' = \left[\varepsilon_1 \middle| S \to G_b, \tilde{S} \to \tilde{G}_b, L \to H_{b1}, \tilde{L} \to \tilde{H}_{b1}\right] \\ \varepsilon_2' = \left[\varepsilon_2 \middle| S \to G_b, \tilde{S} \to \tilde{G}_b, L \to H_{b1}, \tilde{L} \to \tilde{H}_{b1}\right] \end{cases}, \tag{18}$$

where $X \to Y$ denotes the RV change of replacing X with Y.

2) The approximate PDF and CDF of I_b: With the approximation of $\left(\tilde{G}_b + \tilde{H}_{b1}\right)$ as a zero-mean Gaussian RV, we propose to approximate I_b in (17) as another Gaussian RV Q_b, whose mean and variance are

$$\begin{cases} \mu_{Q_b} = \mu_{G_b} + \mu_{H_{b1}} \\ \sigma^2_{Q_b} = \sigma^2_{G_b} + \sigma^2_{H_{b1}} \end{cases}. \tag{19}$$

According to Theorem 2 and Corollary 3, and from (9), (11) and (18), the total error of approximating I_b as Q_b measured by the KS distance between the CDF of I_b and that of Q_b can be upper-bounded by ε as

$$\varepsilon = (\varepsilon_1 + \varepsilon_2) + (\varepsilon_1' + \varepsilon_2'), \tag{20}$$

where $(\varepsilon_1 + \varepsilon_2)$ is the upper bound on the error associated with the approximation of $I_b^{(1)}$ in (6) as a Gaussian RV G_b, and $(\varepsilon_1' + \varepsilon_2')$ is the upper bound on the error associated with the approximation of $G_b + H_{b1}$ in (16) as a Gaussian RV Q_b.

C. The Distribution of I^{mW} in (5)

The study on the approximate distribution of the sum of multiple independent lognormal RVs has been going on for more than five decades [17]-[21]. According to [17]-[18], the sum of multiple independent lognormal RVs can be well approximated by another lognormal RV. However, some recent studies [19]-[21] concluded that the sum of multiple independent lognormal RVs is better approximated by a power lognormal RV, i.e., with the CDF being a power function of $\Phi(\cdot)$. In this paper, we adopt the power lognormal approximation for I^{mW}, which will be explained in the following.

In our case, since each $I_b, b \in \{2, \ldots, B\}$ is approximated by the Gaussian RV Q_b, the sum of $10^{\frac{1}{10}Q_b}$ can be well approximated by a power lognormal RV [19]-[21] expressed as $\hat{I}^{\mathrm{mW}} = 10^{\frac{1}{10}Q}$, where the PDF and CDF of Q can be respectively written as [19]

$$\begin{cases} \text{PDF of } Q: \\ \qquad f_Q(q) = \lambda \Phi^{\lambda-1}\left(\frac{q-\mu_Q}{\sigma_Q}\right) \frac{1}{\sqrt{2\pi\sigma_Q^2}} \exp\left\{-\frac{(q-\mu_Q)^2}{2\sigma_Q^2}\right\}, \\ \text{CDF of } Q:\ F_Q(q) = \Phi^{\lambda}\left(\frac{q-\mu_Q}{\sigma_Q}\right), \end{cases} \tag{21}$$

where the parameters λ, μ_Q and σ_Q are obtained from $\{\mu_{Q_b}\}$ and $\{\sigma^2_{Q_b}\}$. The method to accomplish such task has been well addressed in [19]-[21]. In Appendix B, we provide an example to obtain λ, μ_Q and σ_Q based on [17], [20] and [21].

As a result of (21), the PDF and CDF of $\hat{I}^{\mathrm{mW}}$ can be respectively written as

$$\begin{cases} \text{PDF of } \hat{I}^{\mathrm{mW}}: \\ f_{\hat{I}^{\mathrm{mW}}}(v) = \lambda \Phi^{\lambda-1}\left(\frac{\zeta \ln v-\mu_Q}{\sigma_Q}\right) \frac{\zeta}{v\sqrt{2\pi\sigma_Q^2}} \exp\left\{-\frac{(\zeta \ln v-\mu_Q)^2}{2\sigma_Q^2}\right\}, \\ \text{CDF of } \hat{I}^{\mathrm{mW}}:\ F_{\hat{I}^{\mathrm{mW}}}(v) = \Phi^{\lambda}\left(\frac{\zeta \ln v-\mu_Q}{\sigma_Q}\right), \end{cases} \tag{22}$$

where $\zeta = \frac{10}{\ln 10}$ is a scalar caused by the variable change from $10\log_{10} v$ to $\ln v$.

Finally, we propose that the distribution of I^{mW} can be approximated by that of $\hat{I}^{\mathrm{mW}}$ shown in (22). Note that in this step of approximation, the approximation error is dependent on the adopted approximate distribution of the sum of multiple independent lognormal RVs. We will study such approximation error in our future work. Note that some recent studies [19]-[21] have shown that the error associated with the power lognormal approximation is reasonably small and good enough for practical use.

D. Summary of the Proposed Analysis of the UL Interference Distribution

To sum up, in the following, we highlight the main steps in our proposed microscopic analysis of the UL interference distribution.

- First, for each $b \in \{2, \ldots, B\}$, we use (9) and (11) to check the error $(\varepsilon_1 + \varepsilon_2)$ associated with the approximation of $I_b^{(1)}$ in (6) as a Gaussian RV G_b.
- Second, for each $b \in \{2, \ldots, B\}$, we use (18) to check the error $(\varepsilon_1' + \varepsilon_2')$ associated with the approximation of $G_b + H_{b1}$ in (16) as a Gaussian RV Q_b. Note that the upper bound of the total approximation error of the above two steps is further obtained from (20), without any requirement on *(i)* the shape and/or size of cell coverage areas, *(ii)* the uniformity of UE distribution, and *(iii)* the type of multi-path fading.
- Finally, we approximate I^{mW} in (5) by a power lognormal RV $\hat{I}^{\mathrm{mW}} = 10^{\frac{1}{10}Q}$, where the PDF and the CDF of Q is expressed as (21) with the parameters λ, μ_Q and σ_Q^2 obtained from Appendix B.

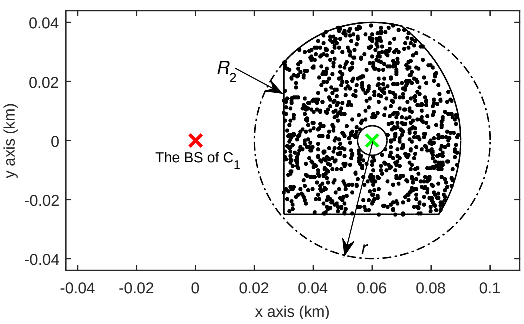

Fig. 2. Illustration of the coverage area R_2 ($r = 0.04\,\text{km}$, uniformly distributed UEs).

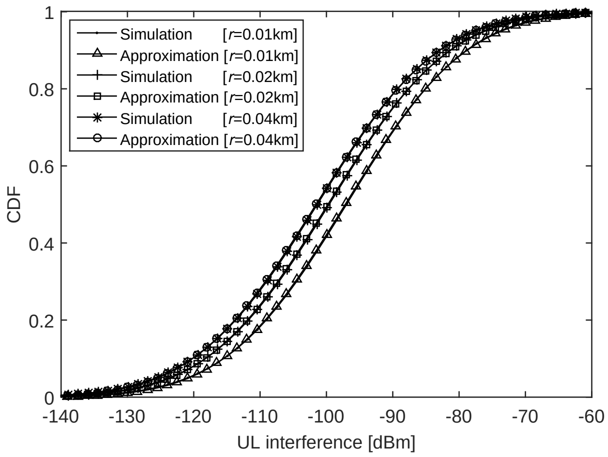

Fig. 3. The simulation and the approximation of the CDF of I_2 ($B = 2$, uniformly distributed UEs, Rayleigh fading).

IV. SIMULATION AND DISCUSSION

In order to validate the approximation from the proposed microscopic analysis of the UL interference, we conduct simulations considering two types of scenarios, i.e., one with a single interfering cell and the other with multiple interfering cells. As discussed in Remarks 1~4 in Subsection III-A1, the parameters for evaluating Theorem 2 and Corollary 3 are set to: $\omega = 0.001$, $p = 4000$, $k_1 = k_2 = 500$. According to the 3GPP standards [14], the system parameters are set to: $A = 103.8$, $\alpha = 20.9$, $P_0 = -76$ dBm, $\eta = 0.8$, and $\sigma_S = 10$ dB. Besides, the minimum BS-to-UE distance is assumed to be 0.005 km [14].

A. The Scenario with a Single Interfering Cell

In this scenario, the number of BSs B is set to 2, and UEs in small cell C_2 are assumed to be uniformly distributed and non-uniformly distributed in the coverage area R_2, respectively.

1) Uniformly Distributed UEs: In this case, we consider uniformly distributed UEs, as shown in Fig. 2. The x-markers indicate BS locations where the BS location of C_1 has been explicitly pointed out. The dash-dot line indicates a reference disk to illustrate the reference size of small cell C_2. The radius of such a reference circle is denoted by r, and the distance between the BS of C_1 and the BS of C_2, i.e., D_2, is assumed to be $1.5r$. The values of r (in km) are set to 0.01, 0.02 and 0.04, respectively [1]. Note that $1.5r$ is just an example and the specific value of D_2 has no impact on the procedure of our analysis.

In this scenario, the interfering UE K_2 is uniformly distributed in an irregularly shaped coverage area R_2, as shown by the area outlined by the solid line in Fig. 2. The shape of R_2 is the intersection of a square, a circle and an ellipse, which has a complicated generation function. Fig. 2 shows examples of the possible positions of K_2 within R_2 as dots. Note that this generation function is just an example and the specific generation function has no impact on the procedure of our analysis.

Despite the complicated shape of R_2, our proposed microscopic analysis of the UL interference distribution still can be applied. Specifically, from Corollary 3, (9), (11), and (18), we can examine the validity of approximating I_2 as a Gaussian RV by checking the corresponding ε given by (20). The results of ε are tabulated for various values of r with the assumption of *Rayleigh fading* in Table II where ε is broken into $(\varepsilon_1 + \varepsilon_2)$ and $(\varepsilon_1' + \varepsilon_2')$. From this table, we can observe that ε_2 and ε_2' are about 100 times larger than ε_1 and ε_1', indicating the dominance of ε_2 and ε_2' in the result of ε. For all the investigated values of r, the values of ε are below 0.01. Consequently, the approximation of I_2 as a Gaussian RV is tight. Note that $r = 0.01$ and $r = 0.02$ correspond to the typical network configurations for future dense and ultra-dense SCNs [1], which shows that our proposed microscopic analysis of the UL interference distribution can be readily used to study future dense and ultra-dense SCNs. Also note that the upper bound ε is much tighter than that presented in our previous work [10]. Specifically, when $r = 0.04$, the upper bound on the approximation error in [10] is around 1.84×10^{-2}, while in Table II ε is around 4.6×10^{-3}.

To further verify the accuracy of the proposed approximation, we plot the simulation results of the CDF of I_2 and the analytical results of the approximate Gaussian CDF according to (19) for the considered R_2 in Fig. 3. Table II also lists the numerical results of μ_{Q_2} and $\sigma_{Q_2}^2$. As can be seen from Fig. 3, the proposed Gaussian approximation of I_2 is tight for the considered R_2 with such an irregular shape. Note that the actual errors between the simulation and the approximation of the CDF of I_2 are also shown in Table II, the results of which establish the validity of the derived upper bound on the approximation error.

To show the approximation errors more clearly at the tail part and the head part in Fig. 3, we use a logarithm scale on the CDF and the complementary CDF (CCDF) of I_2, respectively, and re-plot the results in Fig. 4. Note that such technique is also a common practice of presentation when comparing analytical and simulated CDF curves [17]. As can be seen from Fig. 4, the proposed Gaussian approximation of I_2 is tight for both the tail part and the head part.

As discussed above, Table II is obtained with the assumption of Rayleigh fading. In the following, we will check the approximation errors for Rician fading and another case without multi-path fading. According to [15], a ratio between the

This article has been accepted for publication in a future issue of this journal, but has not been fully edited. Content may change prior to final publication. Citation information: DOI 10.1109/TWC.2016.2538261, IEEE Transactions on Wireless Communications

Table II
APPROXIMATION ERRORS OF THE PROPOSED ANALYSIS ($B = 2$, UNIFORMLY DISTRIBUTED UES, RAYLEIGH FADING).

r	ε	$\varepsilon_1 + \varepsilon_2$	ε_1	$\varepsilon_1' + \varepsilon_2'$	ε_1'	μ_{Q_2}	$\sigma_{Q_2}^2$	Actual error
0.01	4.9×10^{-3}	3.5×10^{-4}	4×10^{-6}	4.6×10^{-3}	4×10^{-6}	-97.1	205.3	1.9×10^{-3}
0.02	5.0×10^{-3}	5.2×10^{-4}	4×10^{-6}	4.5×10^{-3}	4×10^{-6}	-99.7	207.7	1.9×10^{-3}
0.04	4.6×10^{-3}	1.1×10^{-4}	4×10^{-6}	4.5×10^{-3}	4×10^{-6}	-101.5	211.4	1.8×10^{-3}

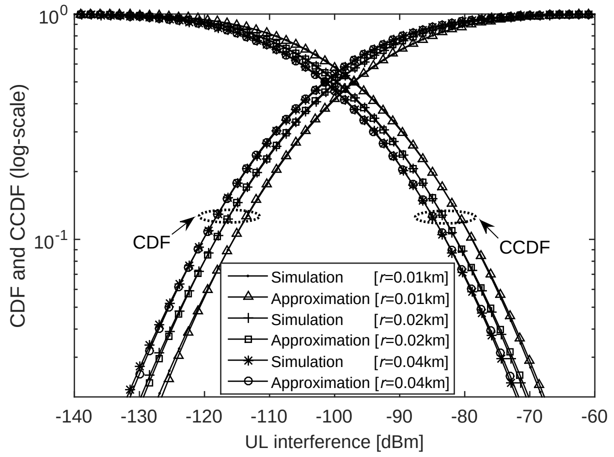

Fig. 4. The simulation and the approximation of the CDF/CCDF of I_2 ($B = 2$, uniformly distributed UEs, Rayleigh fading).

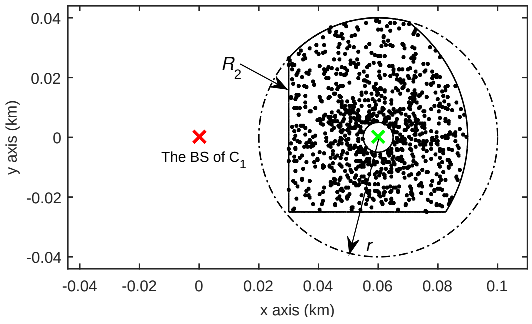

Fig. 5. Illustration of the coverage area R_2 ($r = 0.04$ km, non-uniformly distributed UEs).

power in the line-of-sight (LOS) path and the power in the other scattered paths should be defined for Rician fading. Such ratio is denoted by Γ in our paper. Note that Rician fading will degrade to Rayleigh fading when $\Gamma = 0$. For various values of r under the assumption of Rician fading with $\Gamma = 10$, the results of ε are tabulated in Table III. Comparing Table III with Table II, we can see that the difference lies in the values of $(\varepsilon_1' + \varepsilon_2')$ because they solely depend on the assumption of multi-path fading as discussed in Subsection III-B1. Note that the errors caused by the consideration of Rician fading are actually smaller than those of Rayleigh fading, because Rician fading incurs less randomness due to the dominant LOS path component. Such reduction of randomness in the multi-path fading can be further observed in an extreme case of $\Gamma = +\infty$ where a deterministic LOS path completely dominates the propagation. Table IV shows the results of ε for such extreme case with $\Gamma = +\infty$, i.e., no multi-path fading, where ε_1' and ε_2' are all zeros because the approximation step addressed in Subsection III-B is skipped, rendering $H_{b1} \equiv 0\,\text{dB}$.

For all the investigated values of r, the values of ε are smaller than 0.001 in both Table III and Table IV, indicating that the approximation of I_2 as a Gaussian RV should be even tighter than that observed in Fig. 3. For brevity, we omit these figures. Note that the actual errors between the simulation and the approximation of the CDF of I_2 are provided in Table III and Table IV, the results of which also establish the validity of the derived upper bound ε.

2) Non-Uniformly Distributed UEs: In this subsection, we further investigate the scenario discussed in Subsection IV-A1. Different from previous assumption, here we consider that the interfering UE K_2 is no longer uniformly distributed in R_2. We consider a UE distribution function expressed as $f_{Z_2}(z) = \frac{W}{\rho}, z \in R_2$, where ρ is the radial coordinate of z in the polar coordinate system, the origin of which is placed at the position of the BS of C_2. Besides, W is a normalization constant to make $\int_{R_2} f_{Z_2}(z)\,dz = 1$. In the considered non-uniform UE distribution, UEs are more likely to locate in the close vicinity of the BS of C_2, as shown in Fig. 5, where examples of the possible positions of K_2 within R_2 are shown as dots. Note that the considered $f_{Z_2}(z)$ is just an example of the non-uniformly distributed UEs in R_2, which reflects a reasonable network planning where BSs have been deployed at the center spots of UE clusters. Other forms of the UE distribution function will not affect the procedure of our analysis, only the approximation error values may change with the choice of the UE distribution function. Since we have shown in Subsection IV-A1 that Rayleigh fading is the worst case for the proposed analysis, we adopt such assumption in this subsection.

From (20), we can evaluate the quality of approximating I_2 as a Gaussian RV by checking the corresponding ε. Like Table II, the results of ε for this network scenario are tabulated for various values of r in Table V. As can be seen from Table V, the values of ε are small, i.e., below 0.01, which indicates that the approximation of I_2 as a Gaussian RV is tight, as can be confirmed from the actual error values in Table V.

B. The Scenario with Multiple Interfering Cells

In this subsection, we apply the proposed framework to a more complex network with *practical deployment of multiple cells*, and provide the approximation of the UL interference distribution.

Here, we consider a 3GPP-compliant scenario [14], as shown in Fig. 6, where the number of BSs B is set to 84 and

Table III
APPROXIMATION ERRORS OF THE PROPOSED ANALYSIS ($B = 2$, UNIFORMLY DISTRIBUTED UEs, RICIAN FADING WITH $\Gamma = 10$).

r	ε	$\varepsilon_1 + \varepsilon_2$	ε_1	$\varepsilon_1' + \varepsilon_2'$	ε_1'	μ_{Q_2}	$\sigma_{Q_2}^2$	Actual error
0.01	5.4×10^{-4}	3.5×10^{-4}	4×10^{-6}	1.9×10^{-4}	4×10^{-6}	-95.0	178.2	2.0×10^{-4}
0.02	7.0×10^{-4}	5.2×10^{-4}	4×10^{-6}	1.9×10^{-4}	4×10^{-6}	-97.6	180.8	4.8×10^{-4}
0.04	3.0×10^{-4}	1.1×10^{-4}	4×10^{-6}	1.9×10^{-4}	4×10^{-6}	-99.4	184.5	1.9×10^{-4}

Table IV
APPROXIMATION ERRORS OF THE PROPOSED ANALYSIS ($B = 2$, UNIFORMLY DISTRIBUTED UEs, NO MULTI-PATH FADING).

r	ε	$\varepsilon_1 + \varepsilon_2$	ε_1	$\varepsilon_1' + \varepsilon_2'$	ε_1'	μ_{Q_2}	$\sigma_{Q_2}^2$	Actual error
0.01	3.5×10^{-4}	3.5×10^{-4}	4×10^{-6}	0	0	-94.6	174.2	1.3×10^{-4}
0.02	5.2×10^{-4}	5.2×10^{-4}	4×10^{-6}	0	0	-97.2	176.7	2.4×10^{-4}
0.04	1.1×10^{-4}	1.1×10^{-4}	4×10^{-6}	0	0	-99.0	180.5	0.6×10^{-4}

Table V
APPROXIMATION ERRORS OF THE PROPOSED ANALYSIS ($B = 2$, NON-UNIFORMLY DISTRIBUTED UEs WITH THE DISTRIBUTION FUNCTION OF $f_{Z_2}(z) = \frac{W}{\rho}, z \in R_2$, RAYLEIGH FADING).

r	ε	$\varepsilon_1 + \varepsilon_2$	ε_1	$\varepsilon_1' + \varepsilon_2'$	ε_1'	μ_{Q_2}	$\sigma_{Q_2}^2$	Actual error
0.01	4.9×10^{-3}	4.0×10^{-4}	4×10^{-6}	4.5×10^{-3}	4×10^{-6}	-97.13	205.1	1.8×10^{-3}
0.02	5.3×10^{-3}	7.1×10^{-4}	4×10^{-6}	4.6×10^{-3}	4×10^{-6}	-100.6	207.9	2.2×10^{-3}
0.04	4.9×10^{-3}	4.0×10^{-4}	4×10^{-6}	4.5×10^{-3}	4×10^{-6}	-103.2	214.4	1.7×10^{-3}

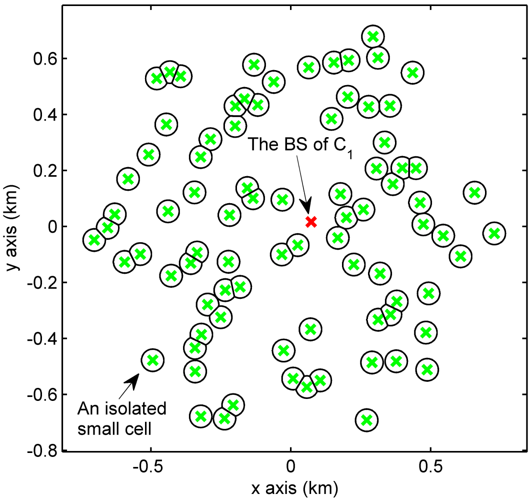

Fig. 6. Illustration of a practical deployment of multiple small cells ($r = 0.04$ km).

all small cell BSs are represented by x-markers. Particularly, the BS of C_1 has been explicitly pointed out. The reference coverage area for each small cell is a disk with a radius of r [14]. As in previous subsections, the values of r (in km) are set to 0.01, 0.02 and 0.04, respectively. The reference disk-shaped areas can be easily seen in Fig. 6 from any isolated small cell. However, due to the irregular positions of the cells, the actual coverage areas of the considered cells are of irregular shapes due to overlapping. The irregularly shaped coverage areas are outlined by solid lines in Fig. 6.

An important note is that the considered network scenario is different from that adopted in [2,3], where coverage areas are defined as Voronoi cells generated by the Poisson distributed BSs, and the *entire* network area is covered by those Voronoi cells. In practice, small cells are mainly used for capacity boosting in specific populated areas, rather than the provision of an umbrella coverage for all UEs [1]. In this light, the 3GPP standards recommend the hotspot scenario depicted in Fig. 6 for UE distribution in the performance evaluation of practical SCNs, and we adopt such network scenario in this subsection. Having said that, we should indicate that the proposed microscopic analysis of the UL interference distribution can still be applied on a particular Voronoi tessellation. This is because Theorem 2 and Corollary 3 in this paper do not rely on particular shape and/or size of coverage areas.

In this subsection, we consider the same UE distribution function as the one discussed in Subsection IV-A2, i.e., $f_{Z_b}(z) = \frac{W}{\rho}, z \in R_b$, where ρ is the radial coordinate of z in the polar coordinate system with its origin placed at the position of the BS of C_b, and W is a normalization constant to make $\int_{R_b} f_{Z_b}(z)\, dz = 1$. Besides, we assume Rayleigh fading in this subsection since Rayleigh fading is the worst case for the proposed analysis as addressed in Subsection IV-A1.

In the following, we investigate the considered network with the proposed microscopic analysis of the UL interference distribution. First, for each $R_b, b \in \{2, \ldots, 84\}$, we invoke (9), (11) and (18) to check the maximum error ε among $b \in \{2, \ldots, 84\}$ using (20). Since the maximum value of ε is reasonably small, e.g., less than 0.01, as shown later, then we can approximate I^{mW} in (5) as a power lognormal RV $\hat{I}^{\mathrm{mW}} = 10^{\frac{1}{10}Q}$, where the PDF and the CDF of Q are given by (21) with the parameters λ, μ_Q and σ_Q^2 obtained from Appendix B.

The maximum values of the 83 R_b-specific ε's for various r values are presented in Table VI. From Table VI, we can observe that, for all the investigated values of r, the

Table VI
APPROXIMATION ERRORS OF THE PROPOSED ANALYSIS ($B = 84$, NON-UNIFORMLY DISTRIBUTED UEs WITH THE DISTRIBUTION FUNCTION OF $f_{Z_b}(z) = \frac{W}{\rho}, z \in R_b$, RAYLEIGH FADING).

r	Max ε	Max $\varepsilon_1 + \varepsilon_2$	Max ε_1	Max $\varepsilon'_1 + \varepsilon'_2$	Max ε'_1	λ	μ_Q	σ^2_Q	Actual error
0.01	5.1×10^{-3}	2.7×10^{-4}	4×10^{-6}	4.8×10^{-3}	4×10^{-6}	48.9	-99.7	116.2	1.73×10^{-2}
0.02	5.1×10^{-3}	4.2×10^{-4}	4×10^{-6}	4.7×10^{-3}	4×10^{-6}	48.0	-101.6	116.5	1.33×10^{-2}
0.04	5.9×10^{-3}	1.2×10^{-3}	4×10^{-6}	4.7×10^{-3}	4×10^{-6}	47.5	-103.1	117.2	1.36×10^{-2}

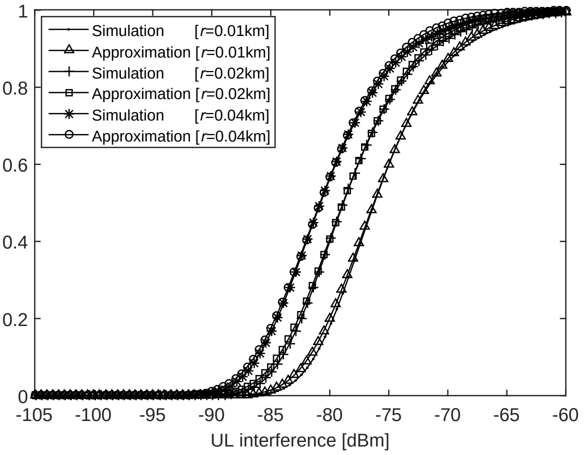

Fig. 7. The simulation and the approximation of the CDF of I^{mW} in dBm ($B = 84$, non-uniformly distributed UEs with the distribution function of $f_{Z_b}(z) = \frac{W}{\rho}, z \in R_b$, Rayleigh fading).

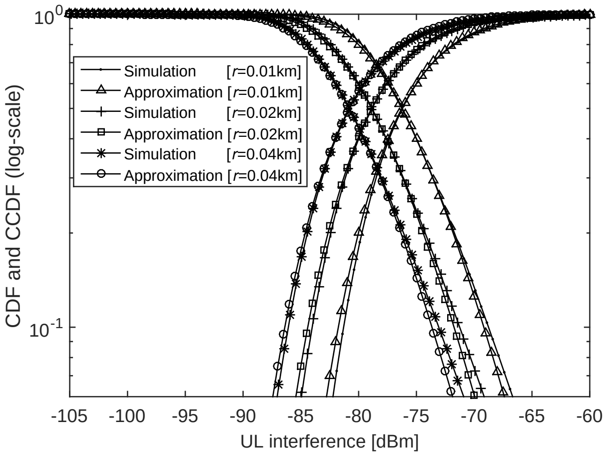

Fig. 8. The simulation and the approximation of the CDF/CCDF of I^{mW} in dBm ($B = 84$, non-uniformly distributed UEs with the distribution function of $f_{Z_b}(z) = \frac{W}{\rho}, z \in R_b$, Rayleigh fading).

maximum values of ε are below 0.01. Thus, each I_b should be well approximated by a Gaussian RV Q_b. Due to space limitation, we omit the detailed numerical investigation on the Gaussian approximation for each I_b, which is very similar to the discussion in Subsection IV-A2. After obtaining the approximation for each I_b, we approximate I^{mW} in (5) as a power lognormal RV $\hat{I}^{\mathrm{mW}} = 10^{\frac{1}{10}Q}$ using (22). The numerical results of λ, μ_Q and σ^2_Q are provided in Table VI for reference.

To further verify the accuracy of our analytical results on the UL interference distribution, in Fig. 7, we plot the simulation results of the CDF of I^{mW} in dBm and the approximate analytical results according to (22). As can be seen from Fig. 7, the resulting power lognormal approximation of I^{mW} is relatively tight with a maximum error around 1.5 percentile (see Table VI). Although the approximate results shown in Fig. 7 should be good enough for practical use, the approximation quality shown in Fig. 7 is not as good as that exhibited in Fig. 3. According to the discussion in Section III, the approximation errors associated with the first and the second steps of approximation are captured in ε, which is very small as can be confirmed from Table VI. The noticeable small approximation errors in Fig. 7 are caused by the inaccuracy of approximating the sum of multiple lognormal RVs as a single power lognormal RV. Note that in our previous work [10], we use a lognormal RV to approximate the sum of multiple lognormal RVs, which lead to even larger errors compared with the results shown in Fig. 7.

To show the approximation errors more clearly at the tail part and the head part in Fig. 7, we use a logarithm scale on the CDF and the CCDF of I^{mW}, respectively, and re-plot the results in Fig. 8. As can be seen from Fig. 8, the power lognormal approximation is slightly tighter at the tail part than the head part when $r = 0.04$, while such approximation is shown to work better at the head part than the tail part when $r = 0.01$. To quantify such approximation error and to find an even better distribution than the power lognormal distribution to approximate the CDF of the sum of multiple lognormal RVs will be our future work.

C. *Discussion on the Complexity of the Proposed Microscopic Analysis*

The computational complexity of the proposed approach is mainly attributable to the numerical integration required to obtain the values of ε for each small cell, which takes standard computers several hours to finish the calculation. In contrast, the simulation approach, e.g., [8], [9] as well as in this paper, involves a tremendously high complexity. Specifically, in our simulations, in order to go through the randomness of all the RVs discussed in Section II, more than *one billion* of realizations of I_b have been conducted for the 83 interfering cells depicted in Fig. 6, which take us several weeks to obtain the results. This shows that the proposed microscopic analysis of network performance is computationally efficient, which makes it a convenient tool to study future 5G systems with general and dense small cell deployments. Moreover, our analytical studies yield better insight into the performance of the system compared with simulations.

This article has been accepted for publication in a future issue of this journal, but has not been fully edited. Content may change prior to final publication. Citation information: DOI 10.1109/TWC.2016.2538261, IEEE Transactions on Wireless Communications

V. CONCLUSION

The lognormal approximation of the UL inter-cell interference in FDMA SCNs is important because it allows tractable network performance analysis. Compared with the existing works, we have analytically derived an upper bound on the error of such approximation, measured by the KS distance between the actual CDF and the approximate CDF.

Our results are general in the sense that we do not pose any requirement on *(i)* the shape and/or size of cell coverage areas, *(ii)* the uniformity of UE distribution, and *(iii)* the type of multi-path fading. Based on our results, we have proposed a new approach to directly and analytically investigate a complex network with *practical deployment of multiple BSs placed at irregular locations*, using the approximation of the aggregate UL interference by a power lognormal distribution. From our theoretical analysis and simulation results, we can see that the proposed approach possesses the following merits:

1) It quantifies the approximation error measured by an upper-bound KS distance using a closed-form function, and the tightness of the approximation is validated by the numerical results.
2) It tolerates more practical assumptions than the existing works, e.g., irregular hot-spots, overlapped cells, etc, and it can cope with a large number of small cells with a low computational complexity of analysis, thus making it a convenient tool to study future 5G systems with general and dense small cell deployments.

As future work, we will further investigate the impact of the correlated shadow fading [27], the three-dimensional (3D) antenna pattern [1] and the multi-antenna transmission [1] on the proposed approximation of the UL interference distribution.

APPENDIX A: PROOF OF THEOREM 2

For clarity, we first summarize our approach to prove Theorem 2 as follows. Our idea is to perform a Fourier series expansion for both the CDF of $\tilde{G}$ and that of the hypothetically approximate Gaussian RV. The distance between those two CDFs will be quantified by the upper-bound KS distance derived in closed-form expressions.

First, according to the definition of $\tilde{G}$, the CDF of $\tilde{G}$ can be formally represented by

$$\begin{aligned} F_{\tilde{G}}(g) &= \Pr\left[\tilde{G} \le g\right] \\ &= \Pr\left[\tilde{L} + \tilde{S} \le g\right] \\ &= \Pr\left[\tilde{S} \le g - \tilde{L}\right] \\ &\triangleq \int_{-\infty}^{+\infty} \Phi\left(\frac{g-l}{\sigma_S}\right) f_{\tilde{L}}(l)\, dl, \end{aligned} \tag{23}$$

where $\Phi(\cdot)$ is the CDF of the standard normal distribution. According to [16], $\Phi\left(\frac{g-l}{\sigma_S}\right)$ can be further written as $\Phi\left(\frac{g-l}{\sigma_S}\right) = 1 - \frac{1}{2}\mathrm{erfc}\left(\frac{g-l}{\sqrt{2}\sigma_S}\right)$, where $\mathrm{erfc}(x)$ is the complementary error function defined as $\mathrm{erfc}(x) = \frac{2}{\sqrt{\pi}}\int_x^{\infty} \exp\left(-t^2\right) dt$ in [15].

Second, due to the independence of $\tilde{L}$ and $\tilde{S}$, the mean and the variance of the approximate Gaussian RV of $\left(\tilde{L} + \tilde{S}\right)$ should be $\mu_{\tilde{L}} + \mu_{\tilde{S}} = 0$ and $\sigma_L^2 + \sigma_S^2$, respectively. As a result, the CDF of such approximate Gaussian RV can be expressed as

$$\Phi\left(\frac{g}{\sqrt{\sigma_L^2 + \sigma_S^2}}\right) = 1 - \frac{1}{2}\mathrm{erfc}\left(\frac{g}{\sqrt{2\left(\sigma_L^2 + \sigma_S^2\right)}}\right). \tag{24}$$

In the following, we will derive the closed-form expressions of the upper-bound KS distance between the two CDFs presented in (23) and (24), respectively.

According to [22], $\mathrm{erfc}(x)$ can be expanded to a Fourier series as

$$\mathrm{erfc}(x) = 1 - \frac{4}{\pi}\sum_{n=1, n\ \text{odd}}^{N=2p-1} \frac{\exp\left(-n^2\omega^2\right)}{n} \sin(2n\omega x) + \delta(x), \tag{25}$$

where ω is the fundamental frequency of the Fourier series, $N = 2p - 1$ is the series truncation point, and $\delta(x)$ is the residual error of the p-truncated Fourier series.

Based on (25), $\Phi\left(\frac{g-l}{\sigma_S}\right)$ in (23) can be expanded as

$$\begin{aligned} &\Phi\left(\frac{g-l}{\sigma_S}\right) \\ &= \frac{1}{2} + \frac{2}{\pi}\sum_{n=1, n\ \text{odd}}^{2p-1} \frac{\exp\left(-n^2\omega^2\right)}{n} \sin\left(2n\omega\frac{g-l}{\sqrt{2}\sigma_S}\right) \\ &\quad - \frac{1}{2}\delta\left(\frac{g-l}{\sqrt{2}\sigma_S}\right) \\ &= \frac{1}{2} + \frac{2}{\pi}\sum_{n=1, n\ \text{odd}}^{2p-1} \frac{\exp\left(-n^2\omega^2\right)}{n} \mathrm{imag}\left\{\exp\left(\mathrm{j}\sqrt{2}n\omega\frac{g-l}{\sigma_S}\right)\right\} \\ &\quad - \frac{1}{2}\delta\left(\frac{g-l}{\sqrt{2}\sigma_S}\right), \end{aligned} \tag{26}$$

where $\mathrm{imag}\{\cdot\}$ extracts the imaginary part of a complex value. Plugging (26) into (23), yields

$$\begin{aligned} F_{\tilde{G}}(g) = &\frac{1}{2} - \frac{1}{2}\int_{-\infty}^{+\infty} \delta\left(\frac{g-l}{\sqrt{2}\sigma_S}\right) f_{\tilde{L}}(l)\, dl \\ &+ \frac{2}{\pi}\mathrm{imag}\left\{\sum_{n=1, n\ \text{odd}}^{2p-1} \exp\left(\mathrm{j}\frac{\sqrt{2}n\omega g}{\sigma_S}\right) \frac{\exp\left(-n^2\omega^2\right)}{n} \right. \\ &\left. \times \int_{-\infty}^{+\infty} \exp\left(-\mathrm{j}\frac{\sqrt{2}n\omega l}{\sigma_S}\right) f_{\tilde{L}}(l)\, dl \right\}, \end{aligned} \tag{27}$$

where the integral $\int_{-\infty}^{+\infty} \exp\left(-\mathrm{j}\frac{\sqrt{2}n\omega l}{\sigma_S}\right) f_{\tilde{L}}(l)\, dl$ is actually the characteristic function [16] of $f_{\tilde{L}}(l)$ evaluated at the point $t = -\frac{\sqrt{2}n\omega}{\sigma_S}$. Such characteristic function, denoted by $\varphi_{\tilde{L}}(t)$, can be written as

$$\varphi_{\tilde{L}}(t) \triangleq \int_{-\infty}^{+\infty} \exp(\mathrm{j}tl) f_{\tilde{L}}(l)\, dl. \tag{28}$$

Hence, from (27) and (28), (23) can be re-formulated as

$$\begin{aligned}
F_{\tilde{G}}(g) &= \frac{1}{2} - \frac{1}{2}\int_{-\infty}^{+\infty} \delta\left(\frac{g-l}{\sqrt{2}\sigma_S}\right) f_{\tilde{L}}(l)\,dl \\
&\quad + \frac{2}{\pi}\mathrm{imag}\left\{\sum_{n=1,n \text{ odd}}^{2p-1} \exp\left(\mathrm{j}\frac{\sqrt{2}n\omega g}{\sigma_S}\right)\right. \\
&\qquad \left. \times \frac{1}{n}\exp\left(-n^2\omega^2\right)\varphi_{\tilde{L}}\left(-\frac{\sqrt{2}n\omega}{\sigma_S}\right)\right\} \\
&= \frac{1}{2} - \frac{1}{2}\int_{-\infty}^{+\infty} \delta\left(\frac{g-l}{\sqrt{2}\sigma_S}\right) f_{\tilde{L}}(l)\,dl \\
&\quad + \frac{2}{\pi}\mathrm{imag}\left\{\sum_{n=1,n \text{ odd}}^{2p-1} \upsilon_n \exp\left(\mathrm{j}\frac{\sqrt{2}n\omega g}{\sigma_S}\right)\right\}, \qquad (29)
\end{aligned}$$

where υ_n is defined as

$$\upsilon_n \triangleq \frac{1}{n}\exp\left(-n^2\omega^2\right)\varphi_{\tilde{L}}\left(-\frac{\sqrt{2}n\omega}{\sigma_S}\right). \qquad (30)$$

And the summation in the imag $\{\cdot\}$ operator of (29) can be deemed as the weighted sum of the unit-amplitude complex values $\left\{\exp\left(\mathrm{j}\frac{\sqrt{2}n\omega g}{\sigma_S}\right)\right\}$, $n \in \{1, 3, \ldots, 2p-1\}$.

Regarding υ_n, by means of the series representation of $\exp(\cdot)$, we can re-write it as

$$\begin{aligned}
\upsilon_n &= \frac{1}{n}\exp\left(-n^2\omega^2\right)\varphi_{\tilde{L}}\left(-\frac{\sqrt{2}n\omega}{\sigma_S}\right) \\
&= \frac{1}{n}\exp\left(-n^2\omega^2\right)\int_{-\infty}^{+\infty}\exp\left(-\mathrm{j}\frac{\sqrt{2}n\omega l}{\sigma_S}\right) f_{\tilde{L}}(l)\,dl \\
&= \frac{1}{n}\exp\left(-n^2\omega^2\right)\int_{-\infty}^{+\infty}\left[1 - \mathrm{j}\frac{\sqrt{2}n\omega l}{\sigma_S} - \frac{1}{2!}\left(\frac{\sqrt{2}n\omega l}{\sigma_S}\right)^2\right. \\
&\qquad \left. + \mathrm{j}\frac{1}{3!}\left(\frac{\sqrt{2}n\omega l}{\sigma_S}\right)^3 + \frac{1}{4!}\left(\frac{\sqrt{2}n\omega l}{\sigma_S}\right)^4 + \cdots\right] f_{\tilde{L}}(l)\,dl \\
&= \frac{1}{n}\exp\left(-n^2\omega^2\right)\left[1 - 0 - \frac{2n^2\omega^2\sigma_L^2}{2\sigma_S^2}\right. \\
&\qquad \left. + \mathrm{j}\frac{\rho_L^{(3)}}{6}\left(\frac{\sqrt{2}n\omega}{\sigma_S}\right)^3 + \frac{\rho_L^{(4)}}{24}\left(\frac{\sqrt{2}n\omega}{\sigma_S}\right)^4 + \cdots\right] \\
&\overset{(a)}{=} \frac{1}{n}\exp\left(-n^2\omega^2\right)\exp\left(-\frac{n^2\omega^2\sigma_L^2}{\sigma_S^2}\right) + \kappa_n \\
&= \frac{1}{n}\exp\left(-n^2\omega^2\left(\frac{\sigma_L^2+\sigma_S^2}{\sigma_S^2}\right)\right) + \kappa_n \\
&= \hat{\upsilon}_n + \kappa_n, \qquad (31)
\end{aligned}$$

where $\hat{\upsilon}_n$ is defined as

$$\hat{\upsilon}_n \triangleq \frac{1}{n}\exp\left(-n^2\omega^2\left(\frac{\sigma_L^2+\sigma_S^2}{\sigma_S^2}\right)\right). \qquad (32)$$

Besides, in (31), κ_n measures the difference between υ_n and $\hat{\upsilon}_n$, defined as $\kappa_n = \upsilon_n - \hat{\upsilon}_n$. The motivation of introducing $\hat{\upsilon}_n$ into (31) is because $\left(1 - \frac{n^2\omega^2\sigma_L^2}{\sigma_S^2}\right)$ can be approximated as $\exp\left(-\frac{n^2\omega^2\sigma_L^2}{\sigma_S^2}\right)$ when $\frac{n^2\omega^2\sigma_L^2}{\sigma_S^2}$ is small in the step (a) of (31). Note that no approximation is assumed in (31) because κ_n fully captures the difference between υ_n and $\hat{\upsilon}_n$.

Plugging (31) and (32) into (29), we can get

$$\begin{aligned}
&F_{\tilde{G}}(g) = \\
&\frac{1}{2} - \frac{1}{2}\int_{-\infty}^{+\infty} \delta\left(\frac{g-l}{\sqrt{2}\sigma_S}\right) f_{\tilde{L}}(l)\,dl \\
&+ \frac{2}{\pi}\mathrm{imag}\left\{\sum_{n=1,n \text{ odd}}^{2p-1} \kappa_n \exp\left(\mathrm{j}\frac{\sqrt{2}n\omega g}{\sigma_S}\right)\right\} \\
&+ \frac{2}{\pi}\sum_{n=1,n \text{ odd}}^{2p-1} \frac{1}{n}\exp\left(-n^2\omega^2\left(\frac{\sigma_L^2+\sigma_S^2}{\sigma_S^2}\right)\right)\sin\left(\frac{\sqrt{2}n\omega g}{\sigma_S}\right). \qquad (33)
\end{aligned}$$

Performing a variable change of $\omega = \bar{\omega}\sqrt{\frac{\sigma_S^2}{\sigma_L^2+\sigma_S^2}}$ in (33), we can obtain

$$\begin{aligned}
&F_{\tilde{G}}(g) = \\
&\frac{1}{2} - \frac{1}{2}\int_{-\infty}^{+\infty} \delta\left(\frac{g-l}{\sqrt{2}\sigma_S}\right) f_{\tilde{L}}(l)\,dl \\
&+ \frac{2}{\pi}\mathrm{imag}\left\{\sum_{n=1,n \text{ odd}}^{2p-1} \kappa_n \exp\left(\frac{\mathrm{j}\sqrt{2}n\bar{\omega} g}{\sqrt{\sigma_L^2+\sigma_S^2}}\right)\right\} \\
&+ \frac{2}{\pi}\sum_{n=1,n \text{ odd}}^{2p-1} \frac{1}{n}\exp\left(-n^2\bar{\omega}^2\right)\sin\left(\frac{\sqrt{2}n\bar{\omega} g}{\sqrt{\sigma_L^2+\sigma_S^2}}\right). \qquad (34)
\end{aligned}$$

On the other hand, from (25), (24) can also be expanded to a Fourier series using $\bar{\omega}$ as

$$\begin{aligned}
&\Phi\left(\frac{g}{\sqrt{\sigma_L^2+\sigma_S^2}}\right) \\
&\quad = \frac{1}{2} - \frac{1}{2}\delta\left(\frac{g}{\sqrt{2\left(\sigma_L^2+\sigma_S^2\right)}}\right) \\
&\quad + \frac{2}{\pi}\sum_{n=1,n \text{ odd}}^{2p-1} \frac{1}{n}\exp\left(-n^2\bar{\omega}^2\right)\sin\left(\frac{\sqrt{2}n\bar{\omega} g}{\sqrt{\sigma_L^2+\sigma_S^2}}\right), \qquad (35)
\end{aligned}$$

where $\delta(\cdot)$ is the residual error function incurred from the p-truncated Fourier series expansion and it has been defined in (25).

From (34) and (35), we can bound the distance between $F_{\tilde{G}}(g)$ and $\Phi\left(\frac{g}{\sqrt{\sigma_L^2+\sigma_S^2}}\right)$ as

$$\begin{aligned}
&\left|F_{\tilde{G}}(g) - \Phi\left(\frac{g}{\sqrt{\sigma_L^2+\sigma_S^2}}\right)\right| \\
&= \left|-\frac{1}{2}\int_{-\infty}^{+\infty} \delta\left(\frac{g-l}{\sqrt{2}\sigma_S}\right) f_{\tilde{L}}(l)\,dl + \frac{1}{2}\delta\left(\frac{g}{\sqrt{2\left(\sigma_L^2+\sigma_S^2\right)}}\right)\right. \\
&\quad \left. + \frac{2}{\pi}\mathrm{imag}\left\{\sum_{n=1,n \text{ odd}}^{2p-1} \kappa_n \exp\left(\frac{\mathrm{j}\sqrt{2}n\bar{\omega} g}{\sqrt{\sigma_L^2+\sigma_S^2}}\right)\right\}\right| \\
&\leq \frac{1}{2}\int_{-\infty}^{+\infty}\left|\delta\left(\frac{g-l}{\sqrt{2}\sigma_S}\right)\right| f_{\tilde{L}}(l)\,dl \\
&\quad + \frac{1}{2}\left|\delta\left(\frac{g}{\sqrt{2\left(\sigma_L^2+\sigma_S^2\right)}}\right)\right| \\
&\quad + \frac{2}{\pi}\sum_{n=1,n \text{ odd}}^{2p-1}\left|\kappa_n\right|. \qquad (36)
\end{aligned}$$

The first two terms in the right-hand side of (36) are caused by the residual errors from the p-truncated Fourier series expansion. From [23], $\delta(x)$ in (25) can be strictly bounded by

$$|\delta(x)| < \frac{2}{\sqrt{\pi}\omega}\operatorname{erfc}((2p+1)\omega) + \operatorname{erfc}\left(\frac{\pi}{2\omega} - |x|\right). \quad (37)$$

Note that such bound is dependent on the value of x, which makes it difficult to handle the first term in the right-hand side of (36), because the integral in that term is computed from $-\infty$ to $+\infty$. Thus, in the following, we will discuss the upper-bound of $|\delta(x)|$ respectively for the case of $|x| \le k$ and for the case of $|x| > k$, where k is a positive scalar.

Considering the monotonic increase of $\operatorname{erfc}\left(\frac{\pi}{2\omega} - |x|\right)$ with respect to $|x|$, we can further bound $|\delta(x)|$ for a range of interest of $|x| < k$ as

$$\begin{aligned} |\delta(x)| &< \frac{2}{\sqrt{\pi}\omega}\operatorname{erfc}((2p+1)\omega) + \operatorname{erfc}\left(\frac{\pi}{2\omega} - k\right) \\ &\triangleq \delta_0(\omega, p, k), \quad (|x| < k). \end{aligned} \quad (38)$$

For the range of $|x| > k$, since $\operatorname{erfc}(x) \le 2$, $|\delta(x)|$ can be bounded by

$$\begin{aligned} |\delta(x)| &< \frac{2}{\sqrt{\pi}\omega}\operatorname{erfc}((2p+1)\omega) + 2 \\ &\triangleq \delta_1(\omega, p), \quad (|x| \ge k). \end{aligned} \quad (39)$$

In order to derive an upper bound that is independent of g for the right-hand side of (36), in the following we consider two cases for g, i.e., $|g| < k_1\sqrt{\sigma_L^2 + \sigma_S^2}$ and $|g| \ge k_1\sqrt{\sigma_L^2 + \sigma_S^2}$, where k_1 is an arbitrary positive scalar.

When $|g| < k_1\sqrt{\sigma_L^2 + \sigma_S^2}$, we can bound the first term in the right-hand side of (36) by

$$\begin{aligned} &\tfrac{1}{2}\int_{-\infty}^{+\infty} \left|\delta\left(\tfrac{g-l}{\sqrt{2}\sigma_S}\right)\right| f_{\tilde{L}}(l)\,dl \\ &< \frac{1}{2}\delta_1(\omega, p) \int\limits_{|l| \ge k_2\sqrt{\sigma_L^2+\sigma_S^2}} f_{\tilde{L}}(l)\,dl \\ &\quad + \frac{1}{2}\delta_0\left(\omega, p, \frac{(k_1+k_2)\sqrt{\sigma_L^2+\sigma_S^2}}{\sqrt{2}\sigma_S}\right) \int\limits_{|l| < k_2\sqrt{\sigma_L^2+\sigma_S^2}} f_{\tilde{L}}(l)\,dl \\ &< \frac{1}{2}\delta_1(\omega, p)\frac{1}{k_2^2} \\ &\quad + \frac{1}{2}\delta_0\left(\omega, p, \frac{(k_1+k_2)\sqrt{\sigma_L^2+\sigma_S^2}}{\sqrt{2}\sigma_S}\right), \end{aligned} \quad (40)$$

where k_2 is another arbitrary positive scalar introduced to facilitate the bounding of the integral from $-\infty$ to $+\infty$ with regard to l. The last step of (40) is valid because (i)

$$\begin{aligned} \int\limits_{|l| \ge k_2\sqrt{\sigma_L^2+\sigma_S^2}} f_{\tilde{L}}(l)\,dl &= \Pr\left[\left|\tilde{L}\right| \ge k_2\sqrt{\sigma_L^2+\sigma_S^2}\right] \\ &\le \Pr\left[\left|\tilde{L}\right| \ge k_2\sqrt{\sigma_L^2}\right] \\ &\le \frac{1}{k_2^2}, \end{aligned} \quad (41)$$

which comes from Chebyshev's inequality [24], and (ii)

$$\int\limits_{|l| < k_2\sqrt{\sigma_L^2+\sigma_S^2}} f_{\tilde{L}}(l)\,dl < \int\limits_{l \in \mathbb{R}} f_{\tilde{L}}(l)\,dl = 1. \quad (42)$$

.

Besides, the second term in the right-hand side of (36) can be bounded by

$$\begin{aligned} &\tfrac{1}{2}\left|\delta\left(\tfrac{g}{\sqrt{2\left(\sigma_L^2+\sigma_S^2\right)}}\right)\right| \\ &\quad < \frac{1}{2}\delta_0\left(\bar{\omega}, p, \frac{k_1}{\sqrt{2}}\right) \\ &\quad = \frac{1}{2}\delta_0\left(\frac{\omega\sqrt{\sigma_L^2+\sigma_S^2}}{\sigma_S}, p, \frac{k_1}{\sqrt{2}}\right). \end{aligned} \quad (43)$$

Plugging (40) and (43) into (36), and considering the definition of ε_1 and ε_2 in (9) and (11), respectively, we can get

$$\begin{aligned} \left|F_{\tilde{G}}(g) - \Phi\left(\frac{g}{\sqrt{\sigma_L^2+\sigma_S^2}}\right)\right| &< \varepsilon_1 + \varepsilon_2, \\ &\left(|g| < k_1\sqrt{\sigma_L^2+\sigma_S^2}\right). \end{aligned} \quad (44)$$

When $|g| \ge k_1\sqrt{\sigma_L^2 + \sigma_S^2}$, we invoke Chebyshev's inequality [24] to obtain

$$\begin{aligned} &\Pr\left[\left|\tilde{G}\right| \ge k_1\sqrt{\sigma_L^2+\sigma_S^2}\right] \\ &= \Pr\left[\left(\tilde{G} \ge k_1\sqrt{\sigma_L^2+\sigma_S^2}\right) \bigcup \left(\tilde{G} \le -k_1\sqrt{\sigma_L^2+\sigma_S^2}\right)\right] \\ &\le \frac{1}{k_1^2}. \end{aligned} \quad (45)$$

Since $\Pr\left[\tilde{G} \ge k_1\sqrt{\sigma_L^2 + \sigma_S^2}\right] = 1 - F_{\tilde{G}}(g)$ and $\left\{\tilde{G} \le -k_1\sqrt{\sigma_L^2 + \sigma_S^2}\right\} \ne \emptyset$, we have

$$1 - F_{\tilde{G}}(g) < \frac{1}{k_1^2}, \quad \left(|g| \ge k_1\sqrt{\sigma_L^2+\sigma_S^2}\right). \quad (46)$$

Therefore, we can bound $\left|F_{\tilde{G}}(g) - \Phi\left(\frac{g}{\sqrt{\sigma_L^2+\sigma_S^2}}\right)\right|$ $\left(|g| \ge k_1\sqrt{\sigma_L^2 + \sigma_S^2}\right)$ by

$$\begin{aligned} &\left|F_{\tilde{G}}(g) - \Phi\left(\tfrac{g}{\sqrt{\sigma_L^2+\sigma_S^2}}\right)\right| \\ &\quad = \left|1 - F_{\tilde{G}}(g) - \left[1 - \Phi\left(\frac{g}{\sqrt{\sigma_L^2+\sigma_S^2}}\right)\right]\right| \\ &\quad \le 1 - F_{\tilde{G}}(g) + \left|1 - \Phi\left(\frac{g}{\sqrt{\sigma_L^2+\sigma_S^2}}\right)\right| \\ &\quad < \frac{1}{k_1^2} + \frac{1}{2}\operatorname{erfc}(k_1), \quad \left(|g| \ge k_1\sqrt{\sigma_L^2+\sigma_S^2}\right), \end{aligned} \quad (47)$$

where (46) and $0 \le 1 - \Phi\left(\frac{g}{\sqrt{\sigma_L^2+\sigma_S^2}}\right) \le \frac{1}{2}\operatorname{erfc}(k_1)$ for $|g| \ge k_1\sqrt{\sigma_L^2 + \sigma_S^2}$, have been plugged into the second last step of (47).

Combining (44) and (47), and considering the definition of ε_3 in (12), we can obtain (8), which concludes our proof.

Appendix B: An Example to Obtain λ, μ_Q and σ_Q

According to [21], with regard to the RV Q, we have

$$\begin{cases} \lim\limits_{q \to +\infty} \frac{\partial \Phi^{-1}(F_Q(q))}{\partial q} = \frac{1}{\sigma_Q} \\ \lim\limits_{q \to -\infty} \frac{\partial \Phi^{-1}(F_Q(q))}{\partial q} = \frac{\sqrt{\lambda}}{\sigma_Q} \end{cases}. \tag{48}$$

Besides, according to [17] and [20], we can get

$$\begin{cases} \lim\limits_{q \to +\infty} \frac{\partial \Phi^{-1}(F_Q(q))}{\partial q} = \frac{1}{\sigma_X} \\ \lim\limits_{q \to -\infty} \frac{\partial \Phi^{-1}(F_Q(q))}{\partial q} = \sqrt{\sum_{b=2}^{B} \sigma_{Q_b}^{-2}} \end{cases}, \tag{49}$$

where σ_X is obtained by solving the following equation set [17]

$$\begin{cases} \hat{\Psi}_X(s_1) = \prod\limits_{b=2}^{B} \hat{\Psi}_{Q_b}(s_1) \triangleq C_1 \\ \hat{\Psi}_X(s_2) = \prod\limits_{b=2}^{B} \hat{\Psi}_{Q_b}(s_2) \triangleq C_2 \end{cases}, \tag{50}$$

where $\hat{\Psi}_X(s)$ is the approximate moment generating function (MGF) evaluated at s for a lognormal RV defined as $10^{\frac{1}{10}X}$. Such approximate MGF is formulated as

$$\hat{\Psi}_X(s) = \sum_{m=1}^{M_0} \frac{w_m}{\sqrt{\pi}} \exp\left(-s \exp\left(\frac{\sqrt{2\sigma_X^2}a_m + \mu_X}{\zeta}\right)\right), \tag{51}$$

where $\zeta = \frac{10}{\ln 10}$, M_0 is the order of the Gauss-Hermite numerical integration, the weights w_m and abscissas a_m for M_0 up to 20 are tabulated in Table 25.10 in [25]. Usually, M_0 is set to be larger than 8 [17]. Similarly, in (50), $\hat{\Psi}_{Q_b}(s)$ is computed by replacing μ_X and σ_X respectively with μ_{Q_b} and σ_{Q_b} in (51). In (50), s_1 and s_2 are two design parameters for generating two equations that can determine the appropriate values of μ_X and σ_X^2. For example, we can choose $s_1 = 0.001$, $s_2 = 0.005$ and $M_0 = 12$ as recommended in [17]. The solution of (50) can be readily found by standard mathematical software programs such as MATLAB. Besides, using μ_X obtained by solving (50), we can match the mean of Q with μ_X to construct a third equation to determine the three parameters, i.e., λ, μ_Q and σ_Q^2, in the power lognormal distribution of Q.

To sum up, based on (48), (49) and matching the mean of Q with μ_X, we have the following equation set to determine the values of λ, μ_Q and σ_Q,

$$\begin{cases} \frac{1}{\sigma_Q} = \frac{1}{\sigma_X} & (a) \\ \frac{\sqrt{\lambda}}{\sigma_Q} = \sqrt{\sum_{b=2}^{B} \sigma_{Q_b}^{-2}} & (b) \\ \int_{-\infty}^{+\infty} q f_Q(q)\, dq = \mu_X & (c) \end{cases}. \tag{52}$$

Note that equations (a) and (b) of (52) are easy to solve and they can deliver λ and σ_Q, while equations (c) of (52) can be efficiently solved by the standard bisection process [26] to determine μ_Q.

References

[1] D. López-Pérez, M. Ding, H. Claussen, and A. H. Jafari, “Towards 1 Gbps/UE in cellular systems: Understanding ultra-dense small cell deployments,” *IEEE Commun. Surveys and Tutorials*, vol. 17, no. 4, pp. 2078-2101, Jun. 2015.

[2] J. G. Andrews, F. Baccelli, and R. K. Ganti, “A tractable approach to coverage and rate in cellular networks,” *IEEE Trans. on Commun.*, vol. 59, no. 11, pp. 3122-3134, Nov. 2011.

[3] T. D. Novlan, H. S. Dhillon and J. G. Andrews, “Analytical modeling of uplink cellular networks,” *IEEE Trans. on Wireless Commun.*, vol. 12, no. 6, pp. 2669-2679, Jun. 2013.

[4] Y. Zhu, J. Xu, Z. Hu, J. Wang and Y. Yang, “Distribution of uplink inter-cell interference in OFDMA networks with power control,” *IEEE ICC 2014*, Sydney, Australia, pp. 5729-5734, Jun. 2014.

[5] S. Singh, N. B. Mehta, A. F. Molisch, and A. Mukhopadhyay, “Moment-matched lognormal modeling of uplink interference with power control and cell selection,” *IEEE Trans. on Wireless Commun.*, vol. 9, no. 3, pp. 932-938, Mar. 2010.

[6] N. B. Mehta, S. Singh, and A. F. Molisch, "An accurate model for interference from spatially distributed shadowed users in CDMA uplinks," *IEEE Globecom 2009*, pp. 1-6, Dec. 2009.

[7] J. He, Z. Tang, H. Chen, and W. Cheng, “Statistical model of OFDMA cellular networks uplink interference using lognormal distribution,” *IEEE Wireless Commun. Letters*, vol. 2, no. 5, pp. 575-578, Oct. 2013.

[8] M. Ding, D. López Pérez, A. V. Vasilakos, and W. Chen, “Dynamic TDD transmissions in homogeneous small cell networks,” *IEEE ICC 2014*, Sydney, Australia, pp. 616-621, Jun. 2014.

[9] M. Ding, D. López Pérez, R. Xue, A. V. Vasilakos, and W. Chen, “Small cell dynamic TDD transmissions in heterogeneous networks,” *IEEE ICC 2014*, Sydney, Australia, pp. 4881-4887, Jun. 2014.

[10] M. Ding, D. López Pérez, G. Mao, and Z. Lin, “Approximation of uplink inter-cell interference in FDMA small cell networks,” *IEEE Globecom 2015*, San Diego, CA, USA, pp. 1-7, Dec. 2015.

[11] 3GPP, “TS 36.213 (V11.2.0): Physical layer procedures,” Feb. 2013.

[12] WiMax Forum, “WiMAX and the IEEE 802.16m Air Interface Standard,” Apr. 2010.

[13] F. J. Massey Jr. “The Kolmogorov-Smirnov test for goodness of fit,” *Journal of the American Statistical Association*, vol. 46, no. 253, pp. 68-78, 1951.

[14] 3GPP, “TR 36.828 (V11.0.0): Further enhancements to LTE Time Division Duplex (TDD) for Downlink-Uplink (DL-UL) interference management and traffic adaptation,” Jun. 2012.

[15] J. Proakis, *Digital Communications (Third Ed.)*, New York: McGraw-Hill, 1995.

[16] I. Gradshteyn and I. Ryzhik, *Table of Integrals, Series, and Products (Seventh Ed.)*, Elsevier Inc., 2007.

[17] N. B. Mehta and A. F. Molisch, “Approximating a sum of random variables with a lognormal,” *IEEE Trans. on Wireless Commun.*, vol. 6, no. 7, pp. 2690-2699, Jul. 2007.

[18] N. C. Beaulieu and Q. Xie, “An optimal lognormal approximation to lognormal sum distributions,” *IEEE Trans. on Vehicular Tech.*, vol. 53, no. 2, pp. 479-489, Mar. 2004.

[19] Z. Liu, J. Almhana, and R. McGorman, “Approximating lognormal sum distributions with power lognormal distributions,” *IEEE Trans. on Vehicular Tech.*, vol. 57, no. 4, pp. 2611-2617, Jul. 2008.

[20] S. S. Szyszkowicz and H. Yanikomeroglu, “On the tails of the distribution of the sum of lognormals,” *IEEE ICC 2007*, Glasgow, Scotland, pp. 5324-5329, Jun. 2007.

[21] S. S. Szyszkowicz and H. Yanikomeroglu, “Fitting the modified-power-lognormal to the sum of independent lognormals distribution,” *IEEE Globecom 2009*, Honolulu, HI, USA, pp. 1-6, Nov. 2009.

[22] C. Tellambura and A. Annamalai, “Efficient computation of erfc(x) for large arguments,” *IEEE Trans. on Commun.*, vol. 48, no. 4, pp. 529-532, Apr. 2000.

[23] V. C. Raykar, R. Duraiswami, and B. Krishnapuram, “Fast weighted summation of erfc functions,” CS-TR-4848, Department of computer science, University of Maryland, College Park.

[24] P. Tchebichef, “Des valeurs moyennes,” *J. de mathématiques pures et appliquées*, vol. 22, no. 2, pp. 177-184, 1867.

[25] M. Abramowitz and I. Stegun, *Handbook of mathematical functions with formulas, graphs, and mathematical tables (Nineth Ed.)*, Dover, 1972.

[26] R. L. Burden and J. D. Faires, *Numerical Analysis (Third Ed.)*, PWS Publishers, 1985.

[27] M. Ding, M. Zhang, D. López Pérez, and H. Claussen, “Correlated shadow fading for cellular networks system-level simulations with wrap-around,” *IEEE ICC 2015*, London, UK, pp. 2245-2250, Jun. 2015.

Ming Ding (M'12) received the B.S. and M.S. degrees (with first class Hons.) in electronics engineering from Shanghai Jiao Tong University (SJTU), Shanghai, China, and the Doctor of Philosophy (Ph.D.) degree in signal and information processing from SJTU, in 2004, 2007, and 2011, respectively. From September 2007 to September 2011, he pursued the Ph.D. degree at SJTU while at the same time working as a Researcher/Senior Researcher Sharp Laboratories of China (SLC). After achieving the Ph.D. degree, he continued working with SLC as a Senior Researcher/Principal Researcher until September 2014, when he joined National Information and Communications Technology Australia (NICTA). In September 2015, Commonwealth Scientific and Industrial Research Organization (CSIRO) and NICTA joined forces to create Data61, where he continued as a Researcher in this new R&D center located in Sydney, N.S.W., Australia. He has authored more than 30 papers in IEEE journals and conferences, all in recognized venues, and about 20 3GPP standardization contributions, as well as a Springer book Multi-point Cooperative Communication Systems: Theory and Applications. Also, as the first inventor, he holds 15 CN, 7 JP, 3 US, 2 KR patents and co-authored another 100+ patent applications on 4G/5G technologies. His research interests include B3G, 4G, and 5G wireless communication networks, synchronization, MIMO technology, cooperative communications, heterogeneous networks, device-to-device communications, and modelling of wireless communication systems. He served as the Algorithm Design Director and Programming Director for a system-level simulator of future telecommunication networks in SLC for more than 7 years. He is or has been Guest Editor/Co-Chair/TPC member of several IEEE top-tier journals/conferences, e.g., the IEEE Journal on Selected Areas in Communications, the IEEE Communications Magazine, and the IEEE Globecom Workshops. For his inventions and publications, he was the recipient of the President's Award of SLC in 2012, and served as one of the key members in the 4G/5G standardization team when it was awarded in 2014 as Sharp Company Best Team: LTE 2014 Standardization Patent Portfolio.

David López-Pérez (M'12) is a Member of Technical Staff at Bell Laboratories, Alcatel-Lucent, and his main research interests are in HetNets, small cells, interference and mobility management as well as network optimization and simulation. Prior to this, David earned his PhD in Wireless Networking from the University of Bedfordshire, UK in Apr. '11. David was Research Associate at King's College London, UK from Aug. '10 to Dec. '11, carrying post-doctoral studies, and was with VODAFONE, Spain from Feb. '05 to Feb. '06, working in the area of network planning and optimization. David was also invited researcher at DOCOMO USA labs, CA in 2011, and CITI INSA, France in 2009. For his publications and patent contributions, David is a recipient of both the Bell Labs Alcatel-Lucent Award of Excellence and Certificate of Outstanding Achievement. He was also finalist for the Scientist of the Year prize in The Irish Laboratory Awards (2013). David has also been awarded as PhD Marie-Curie Fellow in 2007 and Exemplary Reviewer for IEEE Communications Letters in 2011. David is editor of the book "Heterogeneous Cellular Networks: Theory, Simulation and Deployment" Cambridge University Press, 2012. Moreover, he has published more than 70 book chapters, journal and conference papers, all in recognized venues, and filed more than 30 patents applications. David is or has been guest editor of a number of journals, e.g., IEEE JSAC, IEEE Comm. Mag., TPC member of top tier conferences, e.g., IEEE Globecom and IEEE PIMRC, and co-chair of a number of workshops.

Guoqiang Mao (M'02-SM'08) received PhD in telecommunications engineering in 2002 from Edith Cowan University. He currently holds the position of Professor of Wireless Networking, Director of Center for Real-time Information Networks at the University of Technology, Sydney. He has published more than 100 papers in international conferences and journals, which have been cited more than 3000 times. His research interest includes intelligent transport systems, applied graph theory and its applications in telecommunications, wireless sensor networks, wireless localization techniques and network performance analysis.

Zihuai Lin (M'06-SM'10) received the Ph.D. degree in Electrical Engineering from Chalmers University of Technology, Sweden, in 2006. Prior to this he has held positions at Ericsson Research, Stockholm, Sweden. Following Ph.D. graduation, he worked as a Research Associate Professor at Aalborg University, Denmark and currently at the School of Electrical and Information Engineering, the University of Sydney, Australia. His research interests include source/channel/network coding, coded modulation, MIMO, OFDMA, SC-FDMA, radio resource management, cooperative communications, small-cell networks, 5G cellular systems, etc.